

AD-A101 913

JAYCOR ALEXANDRIA VA  
EXPERIMENTAL STUDIES OF AUTOACCELERATION CONCEPTS.(U)  
JUN 81 F SANDEL  
J206-01-006-FR

F/6 20/7

N00173-80-C-0099

NL

UNCLASSIFIED

[inf]

AD 4

10.9.8

END

DATE

FILED

8-81

DTIC

AD A101913

(12)  
B5

LEVEL II

JAYCOR

DTIC  
ELECTED  
JUL 23 1981  
S D  
B

DTIC FILE COPY

DISTRIBUTION STATEMENT A  
Approved for public release  
Distribution Unlimited

205 South Whiting Street  
Alexandria, Virginia 22304

81 6 12 083

(12) LEVEL II

EXPERIMENTAL STUDIES OF  
AUTOACCELERATION CONCEPTS

JAYCOR PROJECT 6193

JAYCOR Report No. J206-01-006-FR  
Contract No. N00173-80-C-0099

June 5, 1981

JAYCOR  
205 S. Whiting Street  
Alexandria, VA 22304

Submitted to:

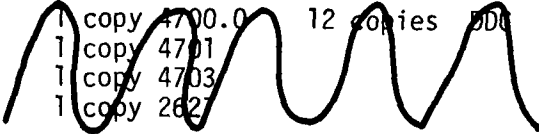
Naval Research Laboratory  
Washington, D.C. 20375

DTIC  
ELECTED  
JUL 23 1981  
S D  
B

DISTRIBUTION STATEMENT A  
Approved for public release;  
Distribution Unlimited

Unclassified

SECURITY CLASSIFICATION OF THIS PAGE (When Data Entered)

REPORT DOCUMENTATION PAGE		READ INSTRUCTIONS BEFORE COMPLETING FORM
1. REPORT NUMBER J206-01-006-FR	2. GOVT ACCESS N NO. AD-A101913	3. RECIPIENT'S CATALOG NUMBER
4. TITLE (and Subtitle) EXPERIMENTAL STUDIES OF AUTOACCELERATION CONCEPTS	5. TYPE OF REPORT & PERIOD COVERED 3/14/80 to 3/14/81	
6. AUTHOR(s) Fredrick Sandel	7. PERFORMING ORG. REPORT NUMBER J206-01-006-FR	
8. PERFORMING ORGANIZATION NAME AND ADDRESS JAYCOR 205 S. Whiting Street Alexandria, VA 22304	9. CONTRACT OR GRANT NUMBER(s) ND0173-80-C-0099	
10. PROGRAM ELEMENT, PROJECT, TASK AREA & WORK UNIT NUMBERS	11. CONTROLLING OFFICE NAME AND ADDRESS Naval Research Laboratory Washington, DC 20375	
12. REPORT DATE June 5, 1981	13. NUMBER OF PAGES 76	
14. MONITORING AGENCY NAME & ADDRESS (if different from Controlling Office) Same as block 11	15. SECURITY CLASS. (of this report) Unclassified	
16. DISTRIBUTION STATEMENT (of this Report)  1 copy 4700.0 1 copy 4701 1 copy 4703 1 copy 262		DISTRIBUTION STATEMENT A Approved for public release; Distribution Unlimited
17. DISTRIBUTION STATEMENT (of the abstract entered in Block 20, if different from Report)		
18. SUPPLEMENTARY NOTES		
19. KEY WORDS (Continue on reverse side if necessary and identify by block number)		
20. ABSTRACT (Continue on reverse side if necessary and identify by block number)		

## TABLE OF CONTENTS

	<u>Page</u>
Overview . . . . .	i
I. Introduction . . . . .	1
II. Diagnostics . . . . .	4
III. Electron beam neutralization . . . . .	8
IV. Backscattered electrons . . . . .	14
V. Potential structure in cavity gaps during the acceleration phase. . . . .	19
VI. 190 $\Omega$ cavity. . . . .	24
VII. Three cavity system results . . . . .	26
VIII. Attempts to reduce neutralization . . . . .	27
IX. Future research on the autoaccelerator. . . . .	30
X. Conclusions . . . . .	32
XI. Appendix . . . . .	34
XII. Figure captions . . . . .	35
Figure 1 through A1 . . . . .	39

### Acknowledgement

This report represents work performed entirely by Dr. T. R. Lockner  
and his colleagues.

Accession For	
NTIS GRA&I	<input checked="" type="checkbox"/>
DTIC TAB	<input type="checkbox"/>
Unannounced	<input type="checkbox"/>
Justification	
<b>PER LETTER</b>	
By _____	
Distribution/ _____	
Availability Codes	
Avail and/or	
Dist	Special
A	

## OVERVIEW

In the past year (Oct 1979 to Sept 1980) significant advances have been made in understanding the physical processes taking place in the Autoaccelerator Experiment. Several new experimental effects have been discovered which explain puzzling results of earlier work, and theoretical support has led to both a clearer understanding of these effects and possible solutions to the problems they produce in the accelerator. In order to put these results in perspective, a short description of our knowledge as of September 1979 would be helpful.

As of September '79 one and two cavity systems had been operated and experimental verification of both the acceleration mechanism and its scaling had been obtained. In the two cavity system it was found that significant emission across the 2nd gap during the acceleration phase limited operation to peak currents below  $\sim 14$  kA. The operation of the 2nd gap could be classified into three regimes. For peak currents below  $\sim 14$  kA the full accelerating voltage appeared across the gap allowing normal operation. For peak currents between  $\sim 14$  and 20 kA emission across the gap caused a decrease of about 10-20% in the accelerating voltage and a slight degradation in the current falltime in the cavity. At current levels above 20 kA the current falltime became extremely long ( $> 100$ ns) and no acceleration was evident. It also became clear from the early experiments that beam alignment was critical to the operation of the two cavity system.

Three experimental observations in these experiments were significant to the following work. First, a probe located in the gap of the 2nd cavity showed evidence of energetic electrons striking the gap during the current risetime. It was found that this electron flux to the wall was present even without the two cavities when the beam was simply propagated down a

drift tube (although at a lower level). Second, during the current risetime the beam became significantly electrostatically neutralized, approaching 50% neutralization at the end of a 600 ns pulse. Third, when the surface area of the anode side of the cavity gap was increased there was a corresponding degradation in the operation of the cavity gap.

These results led to the experimental and theoretical work described in this report. The experimental and theoretical efforts were extremely supportive of one another leading to many cases of theoretical results suggesting new experiments and new experimental results leading to important modifications of theoretical models and parameters. The experimental effort included (listed chronologically):

1. 3 cavity experiments
2. probe measurements of neutral and ion fluxes
3. 190  $\Omega$  cavity experiments
4. discovery of counterstreaming electrons (this is the major electron flux to the wall)
5. mass spectrometer measurements to verify ion flux to the wall
6. attempts to discharge clean the drift tube wall prior to beam propagation
7. attempts to reduce the counterstreaming electron flux
8. energy analysis of electrons striking the wall perpendicular to the surface
9. comparison of the electron flux to the wall versus the number of cavities
10. beam radial position versus electron flux to the wall
11. electron flux to wall versus beam electrostatic neutralization.

The theoretical effort included:

1. modeling of beam neutralization and ion flux to and from the wall using a simple 1-D particle code
2. potential and electric field distributions in the cavity gap versus beam neutralization
3. beam equilibria with neutralization included.

Although significant progress has been made in the past year in understanding the processes involved in the Autoaccelerator, several significant questions have not been answered. Both these questions and possible solutions to the problems of the experiment will be discussed later. Although we have found no "quick-fixes" for the experiment, the success of the basic principle and the knowledge gained through the past year's efforts demonstrate that the concept warrants further pursuit.

## I. INTRODUCTION

The propagation of a long pulse (600-800 ns) electron beam in evacuated drift tube and accelerator gap geometries has been studied. Particular attention has been focused on the drift tube and gap surfaces since formation of plasma here will affect the operation of accelerators such as the Autoaccelerator. Experimental evidence of energetic electron and ion flux to the wall have been obtained. These and other measurements have led to a model describing the spacecharge neutralization of the beam and its effect on accelerator operation.

These studies were initiated because of observations on the Autoaccelerator Experiment. In this experiment an electron beam with a linearly rising current pulse is used to store magnetic energy in coaxial cavities. The cavities are coupled to the beam drift tube via accelerating gaps. When the current is dropped at the end of the beam pulse the stored energy in the cavities is transferred back to a small group of electrons, accelerating them to very high energies. A more detailed description of the Autoaccelerator can be found in the appendix or Reference 1. It was found in the Autoaccelerator that for peak currents above  $\sim 14$  kA, plasma formation at the cavity gap during the current risetime was causing a degradation of the acceleration mechanism at the end of the beam pulse. In addition, energetic electrons were observed at the drift tube wall and electrostatic probe measurements showed substantial electrostatic neutralization of the beam by the end of the pulse. Questions concerning the origin of these effects led to the experiments described in this paper.

There were two primary questions which arose from the Autoaccelerator Cavity experiments. In 2 cavity experiments measurements in the accelerating tap showed that energetic electrons were striking the gap surface during the beam risetime. Damage plates inserted at the end of the cavities

indicated that the primary beam annulus was not intersecting the wall even when energetic electrons were observed in the gap. This observation led to experiments to determine the origin of these energetic electrons.

The second question concerned measurements of the beam electrostatic neutralization as a function of time. Figure 7 shows traces of beam current (a), beam density and electrostatic probe measurement (b) in the drift tube. It is apparent from (b) that the beam becomes significantly electrostatically neutralized late in the pulse. (In this shot the early part of the beam risetime has been sharpened by inserting a series switch between the LC generator and transmission line section. This is done to clarify the timing of all signals. It has no effect on the measurement other than to improve the temporal resolution.)

A description of the diagnostics used in the system is given in Section II. In Section III experimental and theoretical work describing the electrostatic neutralization of the beam is described. Section IV describes the origin and variation of the electron flux to the wall for various experimental setups. The potential structure in the accelerating gaps is described in Section V with the effect of various beam parameters on it. Section VI and VII describe additional cavity experiments performed to clarify the limits on the present total beam acceleration available. Section VIII includes several experimental attempts to reduce the back-scattered electron signal. Section IX lists some future research topics which would be of interest and Section X gives a brief account of our present knowledge of the Autoaccelerator Experiment.

The electron beam and magnetic field configuration is the same as that used for the Autoaccelerator.<sup>1</sup> The electron beam is produced by the foil-less diode configuration shown in Figure 1. An LC generator is connected

to the foilless diode with a quarter cycle risetime of 900 ns. Before the peak of the LC generator pulse a shorting switch fires bringing the diode voltage to zero in  $\sim$  10 ns. Electrons are emitted from a 4.6 cm O. D. annular carbon cathode and accelerated into a 5.0 cm I. D. stainless steel drift tube. Between the drift tube and the anode is a current monitor to measure the portion of the diode current which propagates down the drift tube. The current from this monitor will be referred to as  $I_{DT}$  or  $I_b$  in the future. A typical set of traces of the diode voltage ( $V_D$ ) and drift tube current are shown in Figure 2. Unless otherwise noted the axial magnetic field was held at 10 kG and the field at the cathode had dropped to  $\sim$  8 kG.

## II. DIAGNOSTICS

Standard beam monitors included a Shipman Probe diode voltage monitor in the oil section adjacent to the vacuum interface, a magnetic probe on the diode faceplate to monitor the cathode current and a magnetic probe in the drift tube shielded from the beam to monitor the drift tube current.

Three types of diagnostics were used in the drift tube; electrostatic probes, fast particle detectors and a magnetic spectrometer to measure ion flux to the wall. The electrostatic probes consisted of a vacuum feed-through connector with a wire connected to the center pin to monitor the beam induced electric field as shown in Figure 3. The capacitive coupling of the probe to the beam or wall was small enough so that the signal on the  $50 \Omega$  cable was proportional to  $dE/dt$ . In order to obtain  $E(t)$  the signal was integrated at the scope using a passive RC integrator with a 1 or  $10 \mu s$  RC time. When the probes were installed to measure only the beam spacecharge field, they were recessed outside of the drift tube wall in a 9.5 mm hole  $\sim 2$  mm from the inside edge of the tube. This reduced bombardment of the probe by electrons inside the tube. In some cases the probes were inserted inside the drift tube wall in order to check for the presence of fast electron current striking the wall (Fig. 3). When the probe collected electrons from the drift tube it appeared as a large negative signal superimposed on the normally small ( $\sim 20$  nV) signal due to the beam spacecharge. This latter arrangement suffered from the fact that for small electron fluxes to the probe it was difficult to separate the spacecharge contribution from the electron flux when analyzing the scope traces.

Several types of particle detectors were used in the experiment. In order to measure the electron flux to the wall a probe similar in construction to an electrostatic probe was installed with the tip projecting 0.5 mm into a

3.1 mm hole in the drift tube. A stainless steel screen surrounded the probe with a brass cap as shown in Figure 3. The acceptance angle for this detector was  $\sim 45^{\circ}$ . Because the probe was shielded from the spacecharge field of the beam, it measured only the electron flux striking the probe. The output was displayed unintegrated on the oscilloscope to determine when energetic electrons were arriving at the wall.

In order to obtain an estimate of the energy of the particles striking the wall three probes were placed outside the drift tube at the same axial position with the probe tip  $\sim 0.5$  mm outside the drift tube wall as shown in Figure 3. One of these had a stainless steel screen soldered over the 3.1 mm hole and the other two had .002 and .010 inch stainless shim stock covering them. A comparison of these three probe signals gave a crude estimate of the energy distribution of the electrons bombarding the wall.

Several ion and neutral particle diagnostics were developed to determine the flux of particles to the drift tube wall. The simplest consists of a collector surface at an oblique angle with the axial magnetic field and direction of expected particle flux. Near this surface a wire was positioned to collect the secondary electrons emitted due to particle bombardment. These probes were designed to measure the temporal development of the particle flux to the wall. Two probe designs are shown in Figure 4 and their locations in Figure 5. The probes were shielded from the beam spacecharge field by inserting a conducting screen between the beam and collector. In addition they were recessed at different positions outside the drift tube wall to avoid electron bombardment. The positions of the detectors will be discussed in more detail in the next section.

In order to determine the species and energies of the ions striking the drift tube wall one of the coaxial cavities from the Autoaccelerator

was modified to be used as a magnetic spectrometer. The configuration is shown in Figure 6. A thin stainless steel tube was inserted inside the drift tube to shorten the cavity gap. A 2 mm slit allowed ions which would normally have struck the drift tube wall to pass into the cavity. Once in the cavity they propagate on a cyclotron trajectory which intersects the tube at some angle  $\phi$  with respect to the slit. Assuming the particle has no angular velocity as it passes through the slit (this assumption will be discussed later), and it arrives at the collector at time  $T_A$ , relative to when it passes through the slit, the mass and energy of an ion are given by

$$M_i = \frac{Z_i e B T_A}{M_p} \quad \frac{1}{\phi + \eta} \quad (1)$$

$$E_i = \frac{Z_i B r_w^2}{2 T_A} (\phi + \eta) \tan^2(\frac{\phi}{2}) \quad (2)$$

where  $M_i$  is the ion mass in AMU,  $E_i$  is the energy in eV,  $B$  is the field in Tesla,  $Z_i$  is the charge state of the ion,  $T_A$  is the arrival time in seconds and  $\phi$  is the angular displacement of the collector from the slit in radians. This diagnostic gives an indication of the species and energy of the particles emanating from the drift tube. A limit on the mass and energy of the particles is set by the distance to the outer wall of the cavity. For example an Oxygen ion with an energy greater than 3.5 KeV will strike the wall before completing its trajectory to the drift tube wall.

The ion current was collected by 3 Faraday cups which spanned  $\pi/2$  radians of the inner tube circumference. A large experimental error in the measurement is due to the length of the beam pulse and the size of the collectors. The former causes uncertainty in  $T_A$  and the latter in  $\phi$ . Because of these

uncertainties in the measurement this diagnostic was used mainly to bracket the possible energies and masses of the ions and to corroborate the other ion flux measurement. On several shots the magnetic field was reversed to identify the noise level. On all these shots the noise level proved to be negligible after  $\sim 1 \mu\text{s}$  from the start of the pulse and some signals could be identified shortly after the current fall. These results will be discussed in the following section. Because singly ionized particles were assumed to predominate in the experiment  $Z_i$  was taken as 1 in all of the experimental analyses. The fact that most of the signals from the spectrometer could be identified with singly ionized atoms which were prevalent in the system supported this assumption.

### III. ELECTRON BEAM NEUTRALIZATION

Electrostatic neutralization of the electron beam was first observed in cavity experiments on the Autoaccelerator. It was later determined that even in a simple drift tube configuration beam neutralization occurred starting at  $\sim 100$  ns and increased to  $\sim 50\%$  neutralization at the end of the beam pulse. A typical drift tube shot is shown in Figure 7. Here  $n_e$  is found from  $I_{DT}$  and the beam energy and the electrostatic neutralization fraction ( $f_i$ ) is defined as  $f_i = n_i/n_e$ . The observed electrostatic neutralization of the beam led to the development of a model describing the neutralization process.

Let us assume that during the first 100 ns some ions originating at the wall are accelerated through the beam and into the center of the drift tube. The origin of these first ions is not clear but some possible sources will be discussed later. The ions will propagate towards the center of the drift tube but at some point the self field of the ions will cause them to slow down and eventually reverse the sign of their radial velocity, i.e. they will set up a virtual anode. If the reflected ions propagate through the same electric field on their way back to the beam radius as they did on their way to the virtual anode and the beam density does not change, they will return to the wall with no net energy. Experimentally though it is observed that  $f_i$  increases in time, indicating an increase in the ion density inside the beam annulus. Due to the increase in  $n_i$  the ions will see a larger electric field on their way back to the beam radius than when they were propagating towards the axis. This means they can gain energy and may have net energy when they reach the drift tube wall. If their energy is large enough to produce additional ionization at the wall the process may be unstable leading to the observed increase in the neutralization of the beam with time.

In order to test this hypothesis a 1D computer code was set up which used as an input the experimentally observed electrostatic neutralization. Because the theoretical effort was not supported by the JAYCOR NRL contract, only the results will be listed here. A detailed description of these results will be presented in future publications. Computer simulations and analytical work indicated the following.

1. Because of the variation of  $f_i$  with time, ions originating at the wall return to the wall with energies ranging from 10 to 40 KeV.
2. If ion flux from the wall was allowed from  $t=0$ , the first ions to return to the wall did so at  $\sim 120$  ns, the experimentally observed initiation of measureable neutralization.
3. If the ion flux from the wall was allowed to increase until it reached spacecharge limited flow, the initial neutralization was larger than measured experimentally, but after  $\sim 300$  ns, the neutralization was the same, i.e. late in time the ion flux from the wall was not source limited, but spacecharge limited.
4. When the electron beam density drops at the end of the current pulse, there is a large flux of energetic ions to the wall since they are no longer contained by the potential well of the beam.

The theoretical confirmation of the experimental results gives us added confidence that our present model of the beam propagation is correct. We have done both analytical and computer analysis of the model with ion species including H+, C+, N+, O+, and combinations of H+ and C+ or O+. In the computer simulations, many of the results which verify experimentally measured parameters are relatively insensitive to ion species and initial run parameters. This is also encouraging in that a detailed knowledge of the system parameters is not necessary in order to confirm the model.

One of the first and most significant features of the electrostatic neutralization was the delay in the onset of significant neutralization as measured by the electrostatic probes. This is explained by the model as follows.

The propagation time of an ion from one side of the wall to the other is given by

$$\tau_p = 15 \left( \frac{\mu_i \beta(\tau_c)}{I(\tau_c) \ln \frac{r_w}{r_b}} \right)^{1/2} \text{ ns.} \quad (3)$$

where  $\beta(\tau_c)$  is the beam relativistic beta at time  $\tau_c$ ,  $I$  is the beam current in kA,  $\tau_c$  is the time at which the ion was created at the wall,  $\mu_i$  is the ion mass in AMU, and the propagation time  $\tau_p$  is in nanoseconds. The arrival time at the wall is given by

$$\tau_A = \tau_c + \tau_p \quad (4)$$

and the minimum arrival time is then (assuming  $I = \frac{T}{\tau} I_p$ )

$$\tau_{AM} = 10 \left( \frac{\mu_i T}{I_p \ln \frac{r_w}{r_b}} \right)^{1/3} \text{ ns.} \quad (5)$$

where  $T$  is the pulse length in ns,  $I_p$  is the peak current in kA and  $\beta$  is assumed equal to 0.6 during this phase of the pulse. Several assumptions were made in order to obtain this simple result. The beam is modeled as a delta function current density at  $r = r_b$ , i.e.  $J(r) = I \frac{\delta(r-r_b)}{2\pi r_b}$  where  $r_b$  is the beam radius, the ion transit time from the wall to the beam is assumed small compared with the transit time across the tube since  $r_w - r_b \ll r_w$ , and the ion Larmor radius is assumed large compared with the

tube radius ( $r_{\ell i} \gg r_w$ ) so the trajectories can be approximated by straight line orbits inside the beam annulus. In addition the ion density inside the beam is assumed small enough for the virtual anode to be neglected. This will be true early in time before the ion density has increased to a significant fraction of the beam density. With this assumption the drift velocity of the ion is constant inside the beam annulus.

For a typical set of beam parameters ( $I_p = 20$  kA,  $T = 600$  ns,  $r_w = 2.5$ ,  $r_b = 2.1$ ) this formula gives  $\tau_{AM}$  for  $O^+$  and  $C^+$  as 140 ns and 127 ns respectively. Experimentally, it is observed that this is the time when the electrostatic probes become noisy and the signal from the energetic particle analyzers begins. Figure 7 shows digitized traces of beam current and two energetic particle analyzers, one on the drift tube wall and another on the wall of the cavity 6.5 cm from the drift tube axis as shown in Figure 6. If an appropriate value for  $r_w$  is used in the expression for  $\tau_{AM}$  for the probe on the cavity wall the values for  $\tau_{AM}$  for  $O^+$  and  $C^+$  are 213 and 193 ns respectively. As can be seen from the figures the timing of the signals agree closely with these calculated values.

For the detector on the cavity wall the assumption that  $r_{\ell} \ll r_w$  is clearly unjustified. In fact the larmor radius of ions emerging from the beam early in time should be so small that these ions would not reach this probe. It is believed that this probe is responding to a flux of charge exchange neutrals from the drift tube. Ions accelerated into the beam charge exchange off of the background gas and are then free to drift across the magnetic field to the probe. This is borne out by the fact that as the drift tube pressure is reduced from  $10^{-3}$  to  $10^{-5}$  Torr the signal on this probe drops to zero. The signal on the inner probe also drops with pressure but at  $10^{-5}$  Torr there is a significant level which remains. It is assumed that this represents ions

energetic enough (with large enough Larmor radii) to reach the probe on the drift tube wall.

Although the time delay of the signals on the energetic particle detectors and their amplitude variation with pressure gave strong evidence of the existence of an ion background, a more direct measurement was desired. The magnetic spectrometer measurements gave us this direct confirmation. Figure 8 shows a typical set of magnetic spectrometer traces. Several features of the traces in Figure 8 are noteworthy. When the beam current drops to zero the ions in the virtual anode are no longer contained by the potential well of the beam. They will propagate radially to the wall with various energies depending on their position at the time of the current drop. From the simulation output one can see that the ion flux will be higher at the end of the electron beam current pulse over a short time span ( $\sim 50$  ns). To the spectrometer this flux appears as a large current pulse delayed by the ion transit time in the spectrometer. The pulses on the spectrometer channels can be used to determine the ion species present in the ion cloud at the end of the beam pulse. From equations 1 and 2, ions with masses of  $1.28 \pm 0.6$  (hydrogen),  $12 \pm 1$  (carbon) and  $16 \pm 1$  (oxygen) have been observed. The observation of these pulses is especially important for the light ions with short transit times in the spectrometer because their amplitude is well above the noise level in the system after the beam current fall.

In addition to the observation of these pulses, longer signals have been observed after the noise level had died down with delays corresponding to  $28 + 2$  (silicon),  $13 + 1$  (carbon,  $52 + 3$  (iron) and  $17 + 2$  (oxygen). The observation of  $S_i^+$  in the spectrometer is interesting because it is one of the most consistently observed pulses. The source of the silicon may be the diffusion pump oil vaporized from the diode during each shot.

On many of the spectrometer shots, signals were present which suggested ions with masses ranging from 20 to 50 AMU. Although there are no atoms in the system known to have these mass numbers it is possible that singly ionized molecular states of N<sub>2</sub> or O<sub>2</sub> are present. In addition, doubly ionized states of heavier ions such as iron may be present in the system. Because of these ambiguities the magnetic spectrometer was used primarily to corroborate the existence of an energetic ion flux to the wall.

#### IV. BACKSCATTERED ELECTRONS

One of the procedures involved in the alignment of the electron beam diode involves firing a 200 ns beam into a stainless steel witness plate at the end of the drift tube. In the normal operation of the system this plate is removed and the beam is allowed to follow the magnetic field lines as they diverge at the end of the field coil, thus the beam is deposited on the drift tube wall over a large area at the end of the field coil. It was noted that when a witness plate was used the electrostatic probe signals were driven to very large negative values very early in the beam pulse (within the first 30 ns). When a carbon plug was used to replace the stainless steel damage plate the signal level dropped by a factor of  $\sim 5$  but was still significantly greater than the normal electrostatic signals. When a 1 mm thick tube 2.5 cm in length (hereafter referred to as 1 mm skimmer) was inserted inside the drift tube on the cathode side of the probes the signal did not change. But when the skimmer was placed on the downstream side of the probes the normal electrostatic probe signal was obtained with both the stainless steel and carbon plugs at the end of the tube. From these experimental results we have concluded that there is a significant flux of backscattered primary electrons to the wall of the drift tube.

In order to obtain an estimate of the backscattered electron energy a set of three probes were installed with their tips  $\sim 0.5$  mm outside the drift tube wall as described earlier. The holes to the drift tube were covered with a stainless steel mesh, a 2 mil and 10 mil stainless steel foil respectively. Probe traces for a typical shot with the three probes are shown in Figure 9. Note that a significant fraction ( $\sim 20\%$ ) of the electrons are penetrating the 10 mil foil at the end of the pulse and almost all are penetrating the 2 mil foil during the entire pulse. This indicates that the electrons striking the

wall are practically as energetic as those of the primary beam. This is a puzzling result since the backscattering process should generate a distribution of both energy and perpendicular momentum in the backscattered flux. Another factor which will affect the amplitude of these signals is the angular distribution of the incoming electrons. The electron flux through the screen and especially through the foils will be strongly attenuated for electrons striking the foil obliquely, thus these probes will measure primarily the normal flux to the wall.

For the probe described earlier with its tip protruding into the drift tube surrounded by a screen and capped with a brass plate, the situation is just the opposite. This probe will respond only to electron flux with an angle of incidence  $\sim 45^\circ$  or greater to the normal. With this probe there was a clear difference in measured electron flux when a 1 mm skimmer was placed on either side of the probe. When the skimmer was on the cathode side of the probe (upstream) the signal level was unchanged but when located on the opposite side (downstream) the signal level was drastically reduced. This indicates that most of the electron flux is coming from the end of the drift tube.

It was also found that the skimmer need only be a few millimeters away from the probes before the electron bombardment is observed. This indicates a very short diffusion length and large perpendicular energy for these electrons. The amplitude of the backscattered electron signal was also observed to vary along the length of the drift tube, being smaller at the end of the tube than at the diode. These results lead to the conclusion that some process, such as the electron two-stream instability, is scattering the particles radially with an amplitude that increases with decreasing z.

It can also be seen from Figure 10 that the electron bombardment of the wall is beginning very early in the beam pulse. This may be the origin of the initial ions from the wall referred to earlier. The electron flux to the wall may provide the initial ionization necessary to begin the avalanche process involving the ion bombardment of the drift tube wall. In addition, it has been observed that the electron flux to the wall is affected by the presence of the autoaccelerator cavities, i.e. the flux increases with cavities present. This may explain the continued degradation of the cavity operation as more cavities are added to the system.

Another effect which may be associated with the backscattered electron flux is shown in Figure 11. It was found that there was a current threshold below which no significant ion signal was seen in the shots with the magnetic spectrometer. In the normal drift tube arrangement with the beam expanding to the wall with the magnetic field, this threshold was  $\sim 21$  kA. When a damage plate was installed, however, ion signals were observed at peak currents as low as 7.6 kA.

In order to relate the ion spectrometer signal to the peak current, the signal from channel #2 was integrated from  $t = T$  to  $t = T + 2.5 \mu s$ . The result was then normalized to  $I_p$ . This was done for several methods of terminating the beam and the results are shown in Figure 11. The logarithm of the peak signal from the electron wall flux monitor (Figure 4c) is also plotted. Note that as the electron flux increases for different conditions the current necessary to see a signal on the magnetic spectrometer decreases. Although there is a correlation between the two signals one cannot infer that larger electron flux to the wall will produce a larger  $f_i$ . This was also checked and there was no significant change in  $f_i$  for shots where the beam expanded to the wall compared with shots into a stainless steel damage

plate. This result suggests that late in time the ion flux is not limited by any ion production mechanism. As mentioned earlier, when the plasma density becomes large the ion flux will be determined by spacecharge limited flow. In this regime if the electron flux is contributing to the ion production a change in electron flux would not affect the beam neutralization. The magnitude of the electron flux may however determine how early in the beam pulse the spacecharge limited flow regime is encountered.

If the flux is large enough to measure with the spectrometer only in the spacecharge limited flow regime it explains the observed behavior. When the electron flux to the wall is small it takes a longer time and higher currents to reach the condition for spacecharge limited flow. When the flux is high the condition is met at much lower currents. In both cases, however, the beam neutralization maximizes at  $\sim 50\%$  and it is only the early time behavior which would distinguish the two cases. The accuracy of the neutralization measurement is probably too poor to distinguish between the two.

The fact that backscattered electron flux is observed when the beam is deposited on the drift tube wall at the end of the magnetic field coil leads to another conclusion. In this situation the magnetic field intersects the drift tube wall at an angle of less than  $5^\circ$ . Any primary electrons back-scattered off of the wall in this case will be reabsorbed if they have significant perpendicular energy. This means that the backscattered flux will have a very small  $V_{\perp}$ , thus the scattering process which drives them to the wall must increase  $V_{\perp}$  significantly. This is another indication that the scattering process is due to large radial electric fields caused by some wave process such as an electrostatic two-stream instability since electrons falling through the beam's radial field would have an energy of only a few tens of kilovolts in the perpendicular direction.

A set of probes with tips extending into the drift tube were placed at one axial location to measure the azimuthal variation of the backscattered signal. It was found that there was a strong variation in the signal levels between the probes if the beam was off center. The closer the beam approached the wall, the larger the backscattered signal. This variation made it difficult to interpret the electron wall flux data because, for a given probe position, variations in the beam alignment could cause large variations in the signal amplitudes. Whenever possible experiments involving the electron flux to the wall were done without major movement of the experimental apparatus. This effect also suggests that the scattering of the electrons radially may be due to a wave process since the wave amplitude for beam waves will fall off exponentially from the beam edge to the wall. Such an amplitude variation would lead to a large variation in the scattering as a function of distance from the beam and the observed azimuthal variation in electron flux for an off center beam.

## V. POTENTIAL STRUCTURE IN CAVITY GAPS DURING THE ACCELERATION PHASE

During the acceleration phase of the beam pulse the potential distribution inside the gap and electric field on the surfaces of the gap vary significantly. The electric field is the sum of two components, one due to the space charge of the beam and the other from the accelerating potential across the gap. As the beam current drops the component from the beam is decreasing while that from the acceleration potential is increasing. This is clearly seen from the equation for the gap acceleration potential  $V_g$

$$V_g = Z_c (I_p - I) \quad (6)$$

$$= Z_c I_p (1 - \alpha)$$

where  $\alpha = \frac{I}{I_p}$  is the current fall parameter,  $Z_c$  is the cavity impedance, and  $I_p$  is the beam current propagating as the current fall begins. The potential distribution inside the gap geometry depends on the parameter  $x = \frac{V_g}{\rho} \times 10^{-10}$  where  $\rho$  is the total charge per unit length;

$$\rho = N_e - N_i = \frac{(1-f_i) I_b}{\beta c} \quad x = \frac{V_g \beta c}{(1-f_i) I_b} \quad . \quad (7)$$

Here  $N_e$  and  $N_i$  are the electron and ion density per meter. The parameter  $x$  is a measure of the relative amplitude of the two contributions to the electric field. One is from the accelerating potential across the gap and the other is from the total space charge of the electron beam and neutralizing ion background. Potential plots for several values of  $x$  and two geometries are shown in Figures 12 through 13. The current fall parameter is related to  $x$  through the equation

$$x = \frac{\beta c Z_c}{1-f_i} \quad \left( \frac{1-\alpha}{\alpha} \right) \times 10^{-10} \quad (8)$$

For a given  $Z_c$  and  $f_i$ , the potential distribution (and thus  $\chi$ ) is only a function of the magnitude of the current fall ( $\alpha$ ).

The most important feature of these plots is the sign and magnitude of the electric field on the negative side of the gap. Due to the strong axial magnetic field, any electrons emitted from the cathode surface of the gap are constrained to move only in the  $z$  direction. This means that any electron current between the anode and cathode surfaces of the gap must originate in the thin annular projection of the anode surface on the cathode surface. If the direction of the  $z$  component of the electric field in this area is such that electrons are accelerated back towards the cathode, no current will flow across the gap independent of the gap voltage. If, however, the electric field is such that electrons are accelerated towards the anode, any free electrons will cross the gap, constituting a gap current not associated with the beam. The electric field due to the beam space charge is in the direction to accelerate electrons back to the cathode, whereas the electric field due to the gap voltage is in the opposite direction. The surface on which the electric field changes sign is the 0 potential surface in Figures 12 to 13. Note that as  $\alpha$  decreases (as  $I_b$  decreases and  $V_g$  increases) this surface moves from the cavity wall to the inside of the drift tube. The point where electron current across the gap can begin for a  $70 \Omega$  cavity corresponds to a  $\chi$  of  $1.9 \times 10^{-5}$  in geometry #1 and a  $\chi$  of  $1.5 \times 10^{-5}$  in geometry #2. If there is plasma or any other source of free electrons on the cathode surface, the gap emission will begin at these values of  $\chi$ .

From equation 8 it can be seen that as the beam becomes electrostatically neutralized the  $\alpha$  at which current will begin to flow across the gap increases indicating current flow earlier in the beam falltime. This is shown graphi-

cally in Figures 14 and 15 where  $x$  is plotted vs.  $\alpha$  for several values of  $f_i$  and two cavity impedances. Note that for the higher  $Z_c$  the crossover point ( $x$  value) is at an even higher value of  $\alpha$  indicating earlier emission. As an example consider the value of  $x$  in geometry #1 at which the field opposite the anode surface is about to change sign ( $x = 3.15$ ). For  $Z_c = 70$  and  $f_i = 0$  this will correspond to an  $\alpha$  of 0.5 but for  $f_i = 0.5$  (50% neutralization) it corresponds to an  $\alpha$  of 0.57. For a peak current of 20 kA this means that for  $f_i = 0$  emission can begin at a gap voltage of  $\sim 860$  kV whereas for  $f_i = 0.5$  it can begin at  $\sim 600$  kV.

The magnitude of the current emitted across the gap will depend on the electric field strength on the cathode surface. Figures 16 through 19 illustrate how the axial electric field varies with  $x$  (or  $\alpha$  given  $f_i$ ). The electric field is normalized to the field for  $I_p = 1$  kA and plots for two cavity impedances and geometries are shown. The difference in the two geometries is the radius of curvature corresponding to the  $70 \Omega$  cavity and the small radius to the  $190 \Omega$  cavity.

To find the electric field on the cathode surface from Figures 16-19 for a given  $Z_c$ ,  $I_p$ ,  $\alpha$  and  $f_i$  use  $\alpha$ ,  $f_i$  and  $Z_c$  to find  $x$  and multiply the resulting values of  $E_2$  by the peak current. This plot illustrates how the electric field changes in magnitude and sign as the current falls during the acceleration since increasing  $x$  corresponds to decreasing  $\alpha$  holding  $f_i$  and  $Z_c$  constant. Notice the difference in the plots for the two geometries. The electric field opposite the anode surface is strongly influenced by the radius of curvature in this area. Another important feature is that for a given  $f_i$  the crossover point from negative to positive electric field occurs at a lower  $\alpha$  for the higher impedance cavity. This illustrates how the operation of the  $190 \Omega$  cavity will differ from the  $70 \Omega$  cavity. Not only does the geometry reduce

the negative component from the beam but also the increase in gap voltage for a given  $\alpha$  and  $I_p$  increases the positive component. These effects will lead to emission across the  $190 \Omega$  cavity gap earlier than a corresponding shot in the  $70 \Omega$  cavity. At the current levels of our experiment the fields in the  $190 \Omega$  cavity experiment can even surpass the minimum field for explosive emission. This is the ultimate limit of gap voltage since emission will occur even without a preformed plasma on the surface. The difference in the electric field strengths between the two geometries for the  $190 \Omega$  cavity illustrates how even a small change in the gap structure can modify the emission characteristics of the gap.

The effect of beam neutralization on the gap behavior may explain the observed operation of the second cavity in the 2 cavity Autoaccelerator experiments. At currents below  $\sim 14$  kA the cavity operated normally. For currents between 14-10 kA there was a small increase in the current falltime and a corresponding degradation in the accelerating voltage. For currents above 20 kA the current falltime in the second gap became very large indicating significant plasma in the gap prior to the current fall. Because the rate of rise of the beam current remains relatively constant in the experiment, low  $I_p$  implies short beam pulses. Short beam pulses in turn imply small  $f_i$  as seen in Figure 3. In this case not only will the beam spacecharge field predominate during most of the current fall, but also the gap voltage will be small leading to good operation of the gap.

At intermediate currents ( $14 < I_p < 20$  kA) the beam will be significantly neutralized and the gap voltage will increase to the point where any plasma on the surface of the cathode will begin to emit significant current across the gap. This current will reduce the gap voltage and thus the total acceleration of the system.

At high currents ( $I_p > 20$  kA) an electrostatic probe in the gap showed either a total collapse of the beam electric field ( $f_i = 1$ ) or a large positive signal before the current fall. The large positive signal may be due to ion bombardment of the probe when  $f_i \rightarrow 1$  as described earlier. In either case if  $f_i = 1$  and there is significant plasma on the surface, the emission across the gap will be very large leading to the very slow falltime and negligible acceleration.

These arguments also explain an early result on the Autoaccelerator which was very puzzling at the time. A large doughnut was placed on the anode side of the gap in order to reduce the field enhancement on that surface. This resulted in a significant degradation in the operation of the second cavity which can be explained by the above discussion. Since the doughnut increases the radial extent of the anode surface the  $\alpha$  at which emission could occur between the cathode and anode was significantly reduced. The projection of the anode surface onto the cathode was larger and the value of  $\alpha$  at which the 0 potential surface crosses this projection was larger, thus emission began earlier and the total current was greater. This indicates that the gap surfaces can have a significant effect on the efficiency of the accelerator.

All of these arguments lead to the conclusion that neutralization or plasma buildup on the cathode surface must be avoided if proper gap operation is to be insured. It is important to note however that even if there is plasma or a good electron emitter such as carbon on the cathode surface, the beam spacecharge will inhibit gap emission. This implies that proper gap shaping and low  $f_i$  will lead to better gap operation.

## VI. 190 Ω CAVITY

A high impedance cavity was constructed ( $Z_c = 190 \Omega$ ) in order to determine if the autoaccelerator principle scaled with  $Z_c$  as well as the number of cavities. The cavity OD and ID were 119 and 5 cm respectively with a "snout" on the gap end of the cavity to bring the gap into a uniform field region. The cavity geometry is shown in Figure 20. The cavity was 1.8 m long giving a 12 ns pulse length. Four resistor chains with 17-100  $\Omega$  resistors each were installed in the cavity to bring the cavity Q down to 10. Several gap spacings were used but the most consistent operation was for a gap spacing of 2.5 cm. The alignment of the magnetic field proved to be of crucial importance in the experiment with the best results obtained when the system was aligned after each shot. Future experiments should allow for a more accurate magnetic field alignment procedure.

A typical shot is shown in Figure 21. In this shot  $I_p = 20 \pm 2$  kA and  $\alpha = 0.52 \pm .02$  at 10 ns after the peak current. The x-ray pulse is 7.9 times the value at  $I_p$ . The gap voltage for this shot was  $\sim 1.6$  MV giving a total electron energy of 2 MeV after acceleration. The relative increase in x-ray intensity was predicted as 9.5 but a drop in cavity impedance from 190 to 175 ohms due to the loading of the cavity by the resistor chains will explain this decrease. At this current level the cavity appeared to be operating properly.

When the current was increased above 20 kA the cavity operation deteriorated rapidly. The current fall and electrostatic probe trace became very small leading to a much smaller x-ray pulse. The fact that the drift tube monitor also showed a very slow falltime indicates that there was a large amount of plasma in the drift tube leading to emission across the cavity gap and the gap isolating the drift tube monitor from the drift tube. It is likely that

the plasma formation is due to the pulse length and current level. Both will increase the ion and electron bombardment of the walls as previously described, leading ultimately to the total electrostatic neutralization of the beam and a significant plasma density in the tube. It is important to note however that the cavity operation was normal up to this current level. This means that control of the neutralization by using a shorter pulse or by some other means will probably allow operation of the system at much higher current levels.

## VII. THREE CAVITY SYSTEM RESULTS

A three cavity system was built and installed in order to determine if the effects noted with a two cavity system would be enhanced. Two significant effects were seen in this experiment. The electron flux striking the gap of the third cavity was found to begin consistently at 120 ns in the beam pulse and emission across the gap of the third cavity occurred at even lower current levels than for the two cavity system. The most significant discovery in this experiment was that the electron flux reaching the third gap was not due to the primary beam. A damage plate installed at the end of the third cavity indicated that the beam was well centered and propagating several millimeters from the drift tube wall. This indicates the propagation of the primary beam over long distances ( $\sim 4$  meters) and through three gaps did not introduce gross beam instabilities which would break the beam up. Instead, the electron flux observed at the gap was due to a halo of electrons around the primary beam. From the later drift tube studies it is now believed that these are backscattered electrons originating at the end of the tube and propagating back towards the cathode. If these electrons are the source of the plasma on the cavity gap, then elimination of them could lead to normal operation of the three cavity system.

### VIII. ATTEMPTS TO REDUCE NEUTRALIZATION

Electrostatic neutralization of the Autoaccelerator charging beam can seriously affect the operation of the accelerating gaps. This prompted attempts to reduce or eliminate the neutralization by two means. The first involved the elimination or modification of the surface layer on the drift tube wall. There are three sources of contaminants which will be deposited on the wall. The first is the gas loading of the stainless steel from pumpdown and the residual gas pressure during operation. After pumpdown this will consist of the common atmospheric gases ( $O_2$ ,  $N_2$ ,  $H_2O$ ) but after several shots these will be replaced by whatever gases are released during the shot. The second source is the gases released from the electron beam diode during and after the pulse. Because the insulator is coated with diffusion pump oil during cleaning, these gases will consist of hydrocarbons and silicates as well as vapor of the silicon base diffusion pump oil. The presence of the signal on the mass spectrometer identified as  $Si^+$  testifies to the presence of diffusion pump oil products in the ion cloud during the pulse. The third source of contaminants is the cathode material. After many shots blowoff from the carbon cathode will accumulate in the entire system.

An attempt was made to reduce the contaminants on the wall by discharge cleaning before a shot. An electrode was inserted from the downstream end of the drift tube and was connected to the cathode.

The magnetic field coil was energized with a D.C. supply to produce a 100 Gauss field and a high voltage transformer was connected between the electrodes and drift tube wall. The resulting PIG discharge was observed optically, with the electrostatic probes in the drift tube and by the current drawn from the transformer. Through the plastic and plate one could see that the plasma column filled the full length of the end tube and when

the tube was removed it was uniformly hot over the entire length, indicating relatively uniform energy deposition on the wall. A small pressure change was also evident when the discharge was turned on and off indicating that gases were being driven off of the wall. The function of the discharge was to provide electron bombardment of the wall by the discharge electrons. This releases contaminants such as oil and absorbed gases to be pumped out of the system or ionized and moved to the two ends of the tube at the cathode locations. We were able to strike the discharge even at the system base pressure, indicating normal PIG operation. After several shots, with and without discharge cleaning between shots, no significant difference in the output of the magnetic spectrometer was noted. When  $H_2$  was leaked into the system in an attempt to replace the absorbed gases with  $H_2$ , the pulse corresponding to  $H^+$  was larger but no other significant difference was observed. It is likely that the largest electron flux to the walls occurred at the cathode end of the drift tube and thus the remainder of the tube was not cleaned thoroughly enough. It is also possible that the discharge was not intense enough to thoroughly clean the tube. Further attempts at cleaning the tube wall would be worthwhile.

The second means of reducing the neutralization was to reduce the back-scattered electron signal which may be initiating the ion flux. Two methods were attempted: selective absorption on metal fins and the use of a gas cell for dumping the primary beam. The first method relied on the fact that electrons traveling backwards in the drift tube will rotate at twice the EXB drift velocity of an unneutralized beam. It was reasoned that if long radial fins (i.e. metal plates in planes of constant  $\theta$ ) were inserted just ahead of the damage plate the primary beam would not strike the fins. On the other hand the backscattered electrons, due to their rotation, would strike the plates and be absorbed. A set of carbon fins were installed in front of a stainless

steel damage plate as shown in Figure 22a to see if the backscattered signal was significantly reduced. The signal did not drop and the reason can be deduced from the damage plate shown in Figure 22b. Note that the beam segments are twisted at the edges. When the magnetic field was reversed a mirror image of this pattern was obtained. As the beam passes the fins it produces an electric field normal to the surface. The drift due to this electric field will cause the deformation shown on the damage plate. In addition any backscattered electrons will see this normal field and simply drift perpendicular to the wall. Obviously any structure inserted in the tube will generate a normal electric field which will move the backscattered electrons parallel to the surface.

The second method involved placing a gas cell in front of the damage plate. It was felt that the difference in perpendicular energy in the primary and backscattered beam would preferentially absorb the backscattered beam in the gas cell. Experiments using a 50 cm gas cell at  $\sim$  1 Torr of air before the damage plate reduced the backscattered signal by a factor of 2. Although this was an improvement, time restraints and the small magnitude of the change led us to drop the experiments.

## IX. FUTURE RESEARCH ON THE AUTOACCELERATOR

From the progress made in the past fiscal year there are 4 topics which should be pursued in future work on the Autoaccelerator:

A. Significant improvements in the present operation of the autoaccelerator could be obtained by shaping the accelerator gaps. Potential plots such as those of Figures 12 through 13 should be made of gap geometries in order to enhance the component of the electric field from the beam space charge. Shaping of the electrodes should include the effects on the accelerated beam propagation found in the RADLAC experiment. By proper shaping of the electrodes one may obtain greater gap voltages and significant beam focusing simultaneously.

B. From the results on plasma production on the walls and beam electrostatic neutralization, a shorter charging beam may eliminate many of the gap problems exhibited by the multiple cavity experiments. Reducing the charging beam period to 200 ns will drop  $f_i$  to a negligible value while reducing the plasma production on the wall. In order to confirm this prediction, drift tube studies with a short pulse beam would be very helpful.

C. If the backscattered electrons are a significant source of the wall plasma, reduction or elimination of this flux should be pursued. This is another area where drift tube studies would be helpful.

D. Further studies of the neutralization process in multiple cavity systems would be of value in determining the source of the multicavity problems. Probe measurements on the cathode side of the acceleration gap should be made to determine if there is an enhanced ion and electron flux to the wall at this location. The effect of multiple cavities on this flux would also be helpful in determining the mechanism responsible for gap breakdown in the multiple cavity experiments.

Although our understanding of the processes occurring in the Auto-accelerator has improved dramatically, a detailed knowledge of the complete physical picture has not been obtained. We especially lack knowledge of the specific process responsible for the scattering of electrons to the wall and the effect the gap has on this process. With this knowledge the Auto-accelerator principle might well be developed into a viable and scalable high energy accelerator.

## X. CONCLUSION

A long pulse intense electron beam propagating in a strong axial magnetic field has been studied. Significant electrostatic neutralization ( $f_i \sim 0.5$ ) has been observed with electrostatic probes and the presence of an ion background at the end of the pulse verified by magnetic spectrometer experiments. The drift tube wall is being bombarded by energetic electrons and ions during the beam risetime and these electrons and ions fluxes may provide the ions at the wall necessary to neutralize the beam. A model has been developed which explains the ion bombardment during the beam pulse. The source of the electron flux to the wall of the drift tube appears to be from the end of the tube with electrons inside the drift tube rapidly diffusing radially to the wall over the entire length of the experiment. The magnitude of the electron flux is strongly influenced by the material used to dump the beam and the geometry of the beam dump.

Our present picture of the neutralization process is as follows. Ions generated at the drift tube wall by backscattered electrons or some other process are accelerated into the beam annulus. These ions first appear back at the wall after  $\sim 120$  ns depending on their atomic mass. They arrive at the wall with sufficient kinetic energy to lead to greater ion production at the wall, thus increasing the fractional neutralization  $f_i$ . Both the ion flux and  $f_i$  increase until limited by the ion spacecharge at the wall. This leads to a limit of  $\sim 50\%$  spacecharge neutralization of the beam. For long pulses and high beam current the ion and electron flux can generate a large enough plasma density at the cavity gap to allow significant emission across the gap during the acceleration phase of the beam pulse. The plasma density can become large enough to propagate into the beam causing total spacecharge neutralization and a corresponding degradation in the gap operation.

Potential plots of the gap region explain several phenomena observed in the Autoaccelerator Experiment and are strongly influenced by the gap geometry and beam electrostatic neutralization. Significant improvement of gap operation can be expected by proper shaping of the cathode surface of the gap.

Several factors indicate that a shorter beam pulse would improve the operation of the Autoaccelerator including:

1. Lower  $f_i$
2. less plasma formation
3. less ion bombardment during the beam falltime
4. higher beam  $\gamma$  for a given beam energy.

We would like to thank Dr. Wahab Ali and Dr. Bruce Miller for helpful discussions concerning these results.

## XI. APPENDIX

The acceleration method is depicted in Figure A1. An annular electron beam is propagated along a strong axial magnetic field through coaxial cavities (A1a). The beam current ( $I_b$ ) rises linearly over a time  $T$  to a peak value  $I_p$  then falls to a value  $I_m$  (A1c). For a time  $\tau_c$  after time  $T$  (A1d) an accelerating potential appears across the gap ( $V_g$ ) given by

$$V_g = (I_p - I_m) z_c = I_p(1 - \alpha)z_c$$

where  $z_c$  is the cavity impedance and  $\alpha$  is the current fall parameter  $\alpha = I_b/I_p$  for  $t > T$ . Since the accelerating voltage appears during and after the current fall there is automatic synchronization between this voltage and the electrons propagating after time  $T$ . The transmission line equivalent of the cavity after time  $T$  is shown in A1e. Note that if current flows across the gap during the acceleration phase ( $T+$ ) it will flow in the opposite direction of the beam current. This will lower  $V_g$  and the energy of the accelerated electrons.

## XII. FIGURE CAPTIONS

1. Autoaccelerator experimental layout. For the drift tube studies the cavities at the right were replaced by a 2 in o.d. stainless steel drift tube.
2. Typical diode voltage (1) and drift tube current (2) traces. Voltage -100 kV per division, current -5 kA per division.
3. Probes: a. electrostatic with probe tip recessed to avoid particle (especially electron) bombardment, b. combined electrostatic and particle detector with probe tip extended into the drift tube to detect electron flux reaching the wall, c. electron flux detector with shield to eliminate electrostatic pickup from the beam, d. probe array to detect electron flux to the wall (1) screen shield (2) 2 mil stainless steel foil attenuator (3) 10 mil stainless steel attenuator.
4. Two biased particle detectors. Particles striking the oblique surface will generate secondary electrons which are collected by the collector surface.
5. Experimental setup for particle detectors to measure ion and neutral flux to the walls. (a) outer probe (b) inner probe (c) Idt.
6. Cavity modified to act as a magnetic spectrometer. (a) Side view showing stainless steel insert with slit for spectrometer aperture. (b) End view showing collector cup positions relative to the aperture slit.
7. Digitized traces of (a) voltage (1) and drift tube current (2), (b) electron density (1) and electrostatic probe trace (2), (c) particle detector output

from Figure 5b (1) and Figure 5a (2), (d) fractional neutralization (1) and ion density (2) calculated from (b). Vertical scales are: a1. 100 kV per div, a2. 2 kA per div, b1. 5E13 electrons per meter div, b2. 0.1 per div, d1. 2E13 ions per meter per div.

8. Magnetic spectrometer output. Numbers denote channels, "A" shows duration of beam pulse. Timescale is 0.5  $\mu$ s per division.
9. Electron wall flux measurement using setup shown in 3d. (a) diode voltage at 100 kV per division, (b) drift tube current at 2 kA per division, (c) detector with screen over hole (note the change in sign of the signal when the beam current drops, this is probably due to the ion flux to the wall at the end of the pulse), (d) detector with 2 mil stainless foil over hole, (e) detector with 10 mil stainless foil over hole. Traces c, d, and e are at the same sensitivity (20 mV/div.).
10. Digitized traces of current (1) and probe as in Figure 3b (2) to show timing of backscattered electrons relative to beam current. Note that electron flux to the wall begins only 30 ns after the beam pulse.
11. Comparison of magnetic spectrometer output with backscattered electron flux with various drift tube beam terminations. X's give the integral of the magnetic spectrometer trace times  $10E6/I_p$ . O's give the loss of the backscattered electron flux/ $I_p$ . Note that as the atomic number of the beam dump increases, the backscattered flux and ion flux also increase.
12. Potential plots for various beam current falls for a geometry with a radiused anode surface. (Geometry #1).

13. Potential plots for various beam current falls for a geometry with a non radiused anode surface. (Geometry #2).
14. Plots of chi versus alpha for a 70 ohm cavity with various fractional neutralization parameters.
15. Plots of chi versus alpha for a 190 ohm cavity with various fractional neutralization parameters.
16. Plots of electric field normalized to peak current versus radius at the anode surface of the cavity for various values of the parameter chi.  
Chi is: a-8.4, b-4.9, c-3.15, d-2.1, e-1.4. Cavity impedance = 70 ohms  
and the plots are for geometry #1.
17. Same as 16 except the cavity impedance is 190 ohms.
18. Same as 16 except the plot is for geometry #2.
19. Same as 16 except the plot is for geometry #2 with a cavity impedance of 190 ohms.
20. 190 ohm cavity experimental layout.
21. Traces from 190 ohm cavity run. (a) diode voltage, (b) drift tube current: upper trace 200 ns per division, lower trace 10 ns per division triggered on current fall, (c) cavity current: timescales are the same as b except the upper and lower traces are reversed, (d) electrostatic probe measuring the gap voltage: 10 ns per division, (e) X-ray output from the beam dump: note that the pulse from the accelerated electrons is approximately 7 times the peak primary beam signal.
22. (a) Arrangement of fins to reduce backscattered electron flux. (b) Sketch of damage plate after a shot with the fins installed.

A1. The principle of the autoaccelerator. (a) the beam propagates through coaxial cavities, (b) the beam current has a slow risetime ( $T$ ) and a fast falltime ( $T+$ ), (c) injected beam voltage, (d) cavity gap voltage, (e) equivalent transmission line circuit of the beam-cavity system after  $t=T$ .

Figure 1

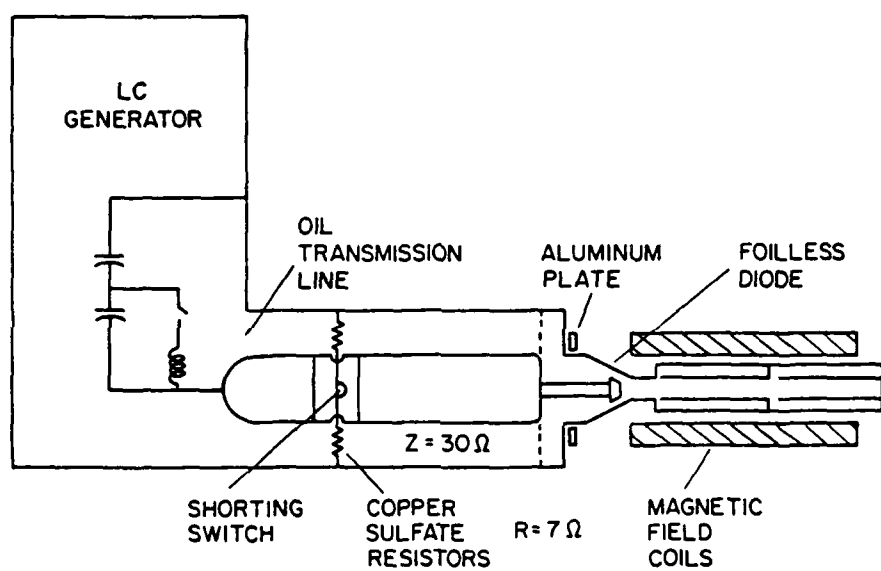


Figure 2

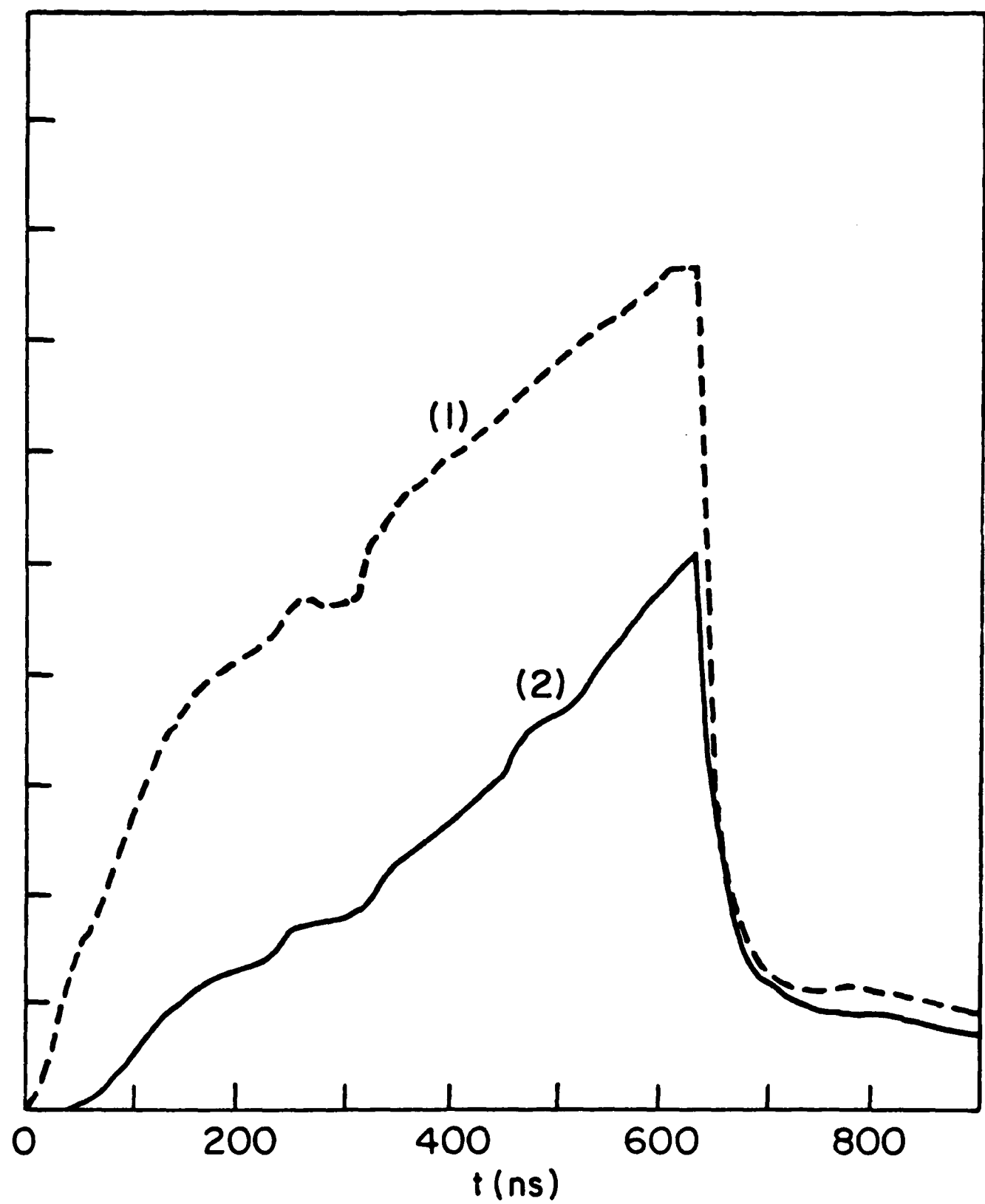


Figure 3

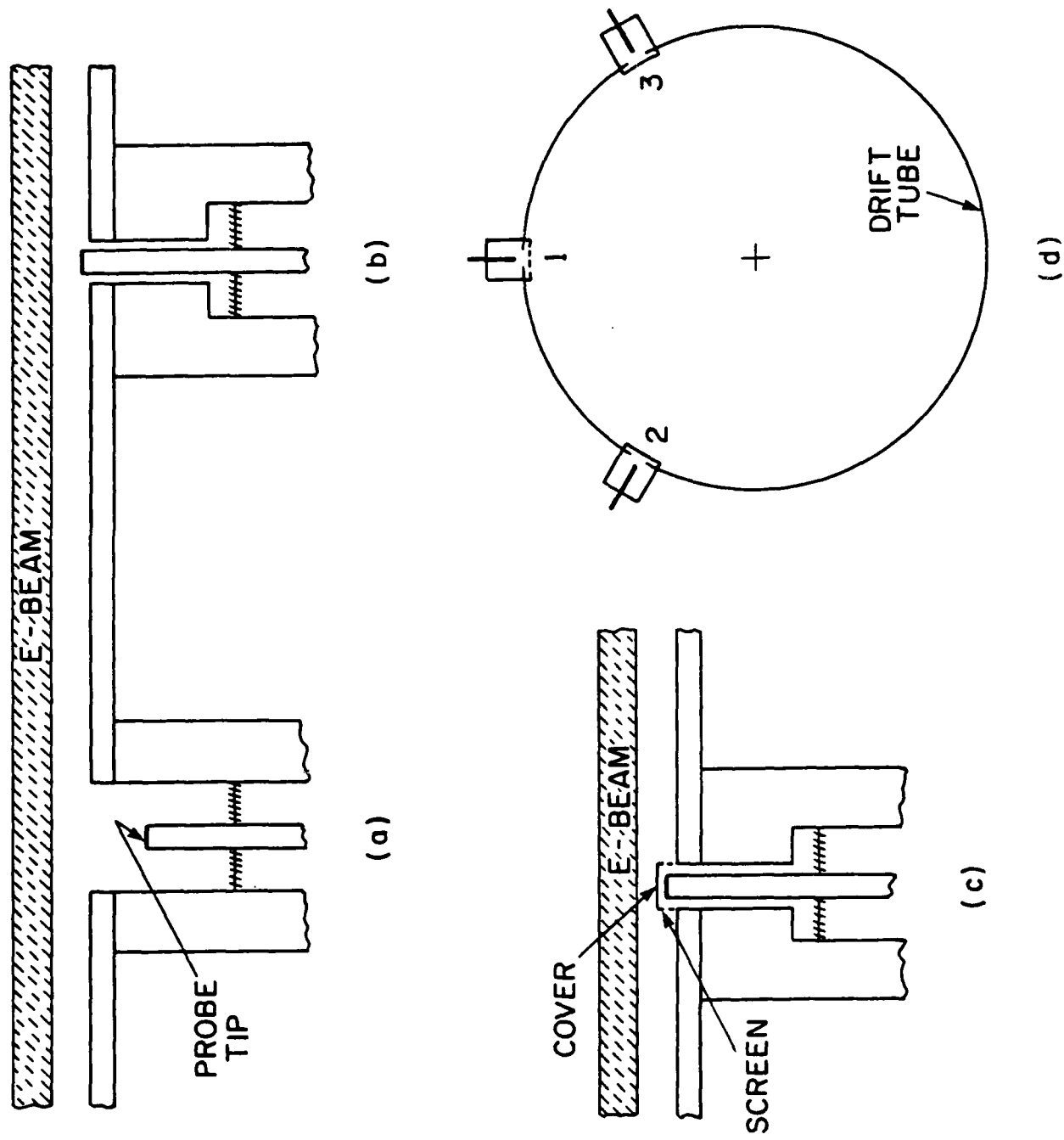


Figure 4

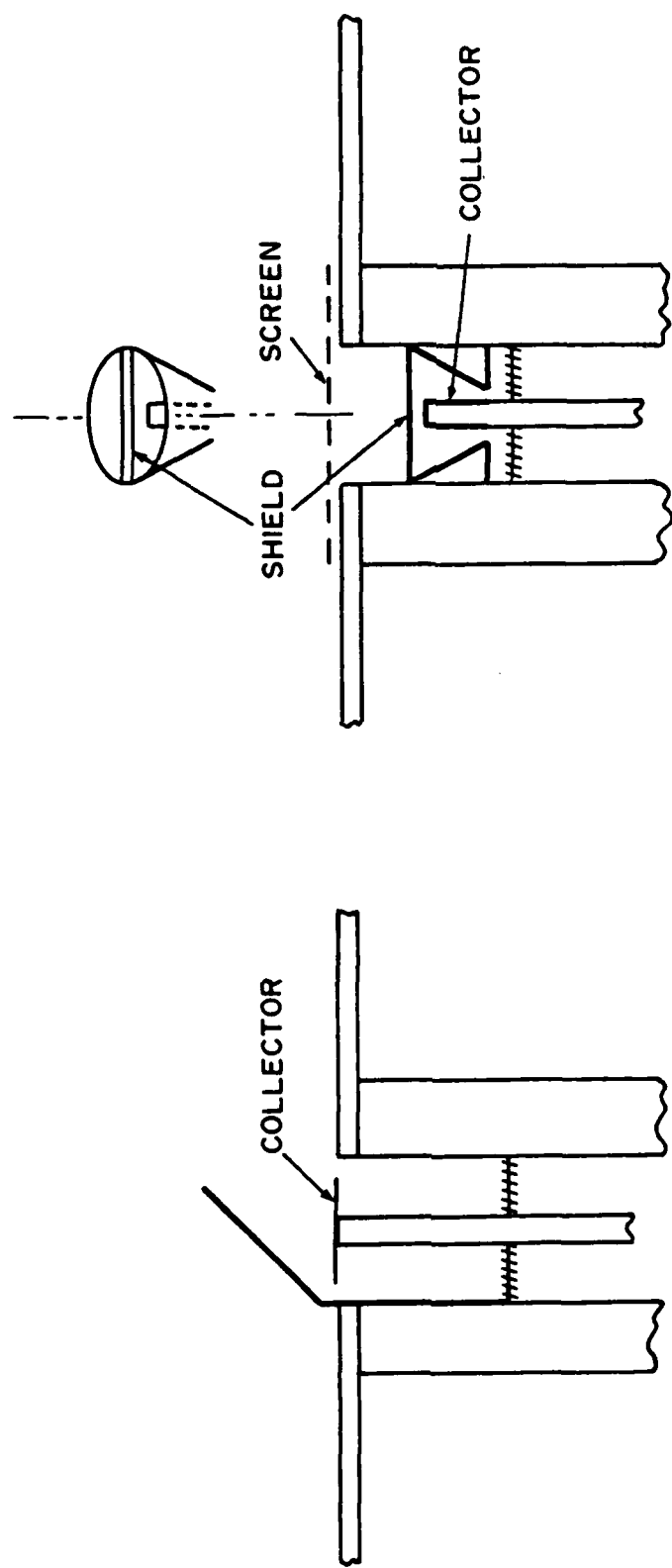


Figure 5

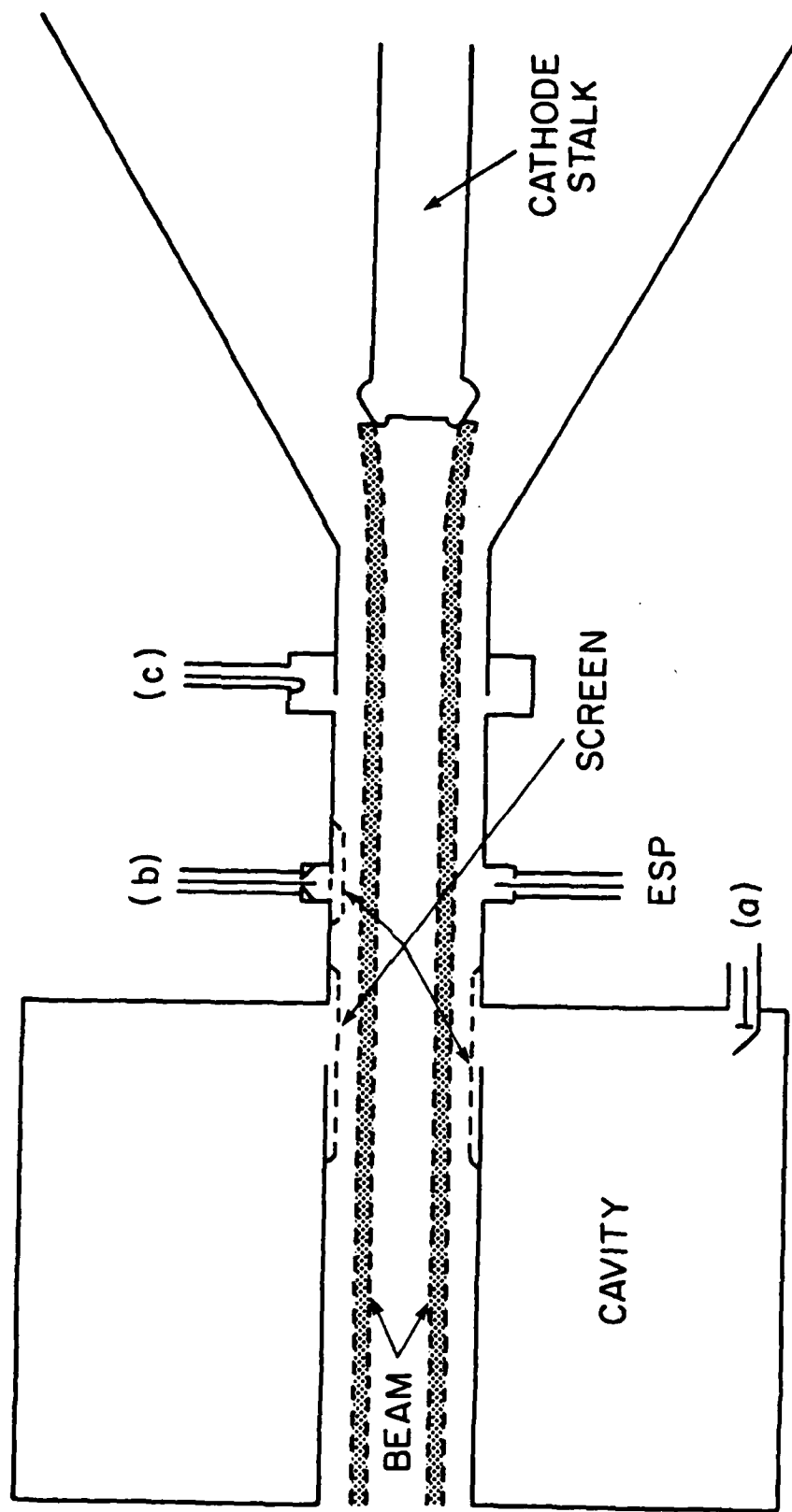


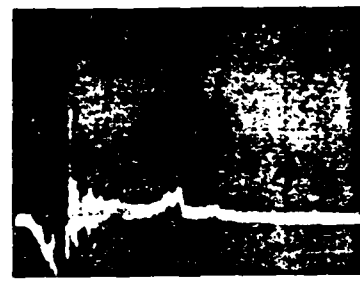
Figure 8



(1)



(2)



→(A)← (3)

Figure 6

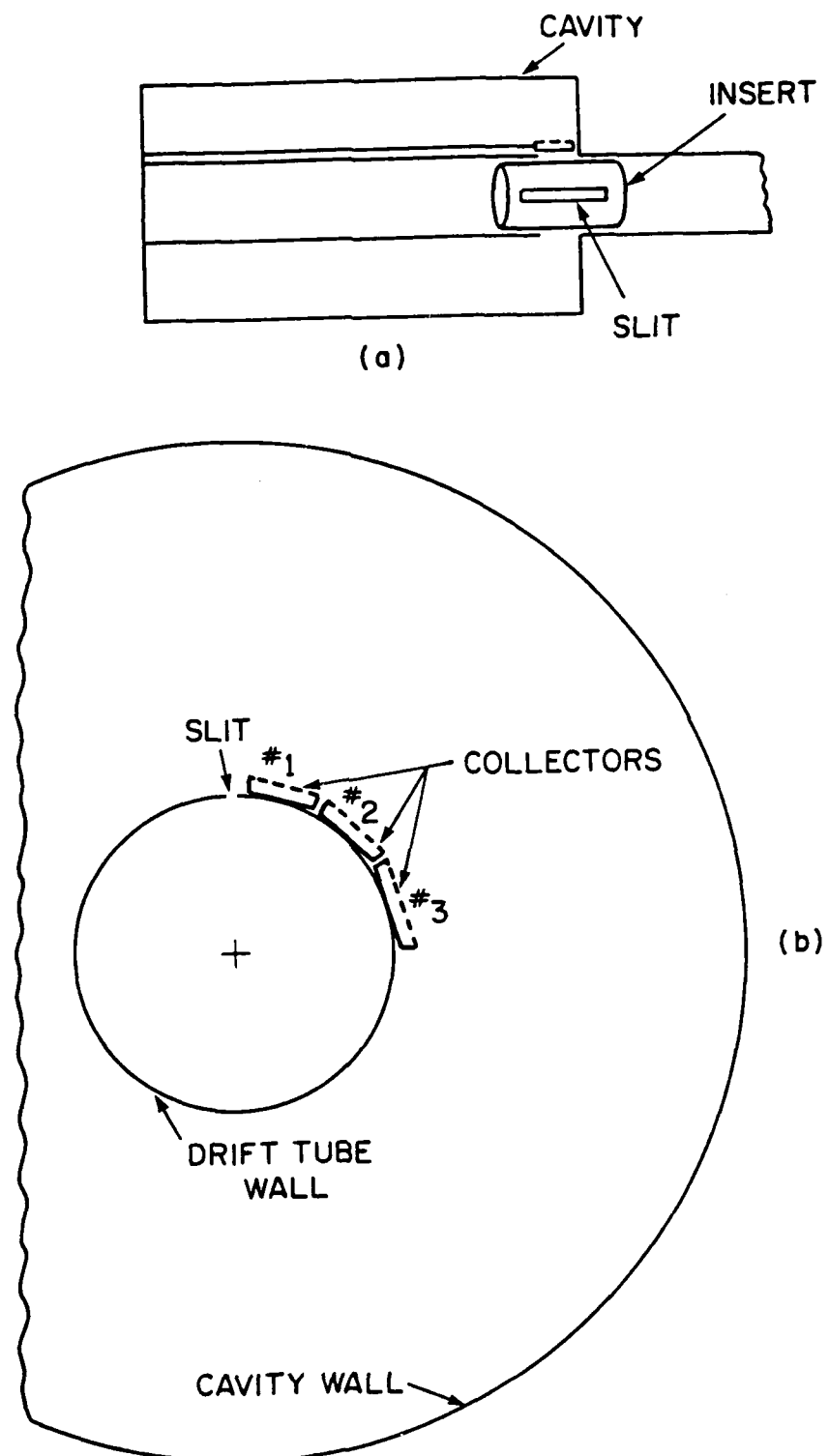


Figure 7

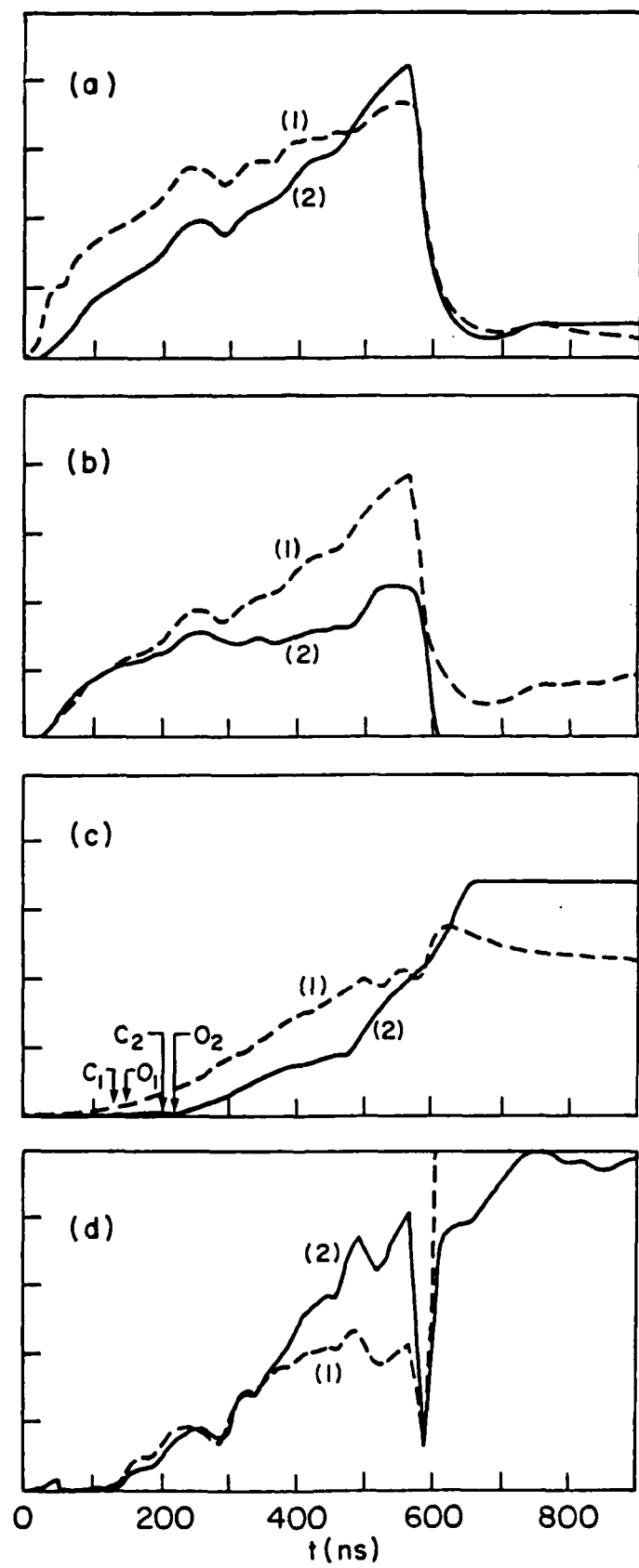


Figure 9

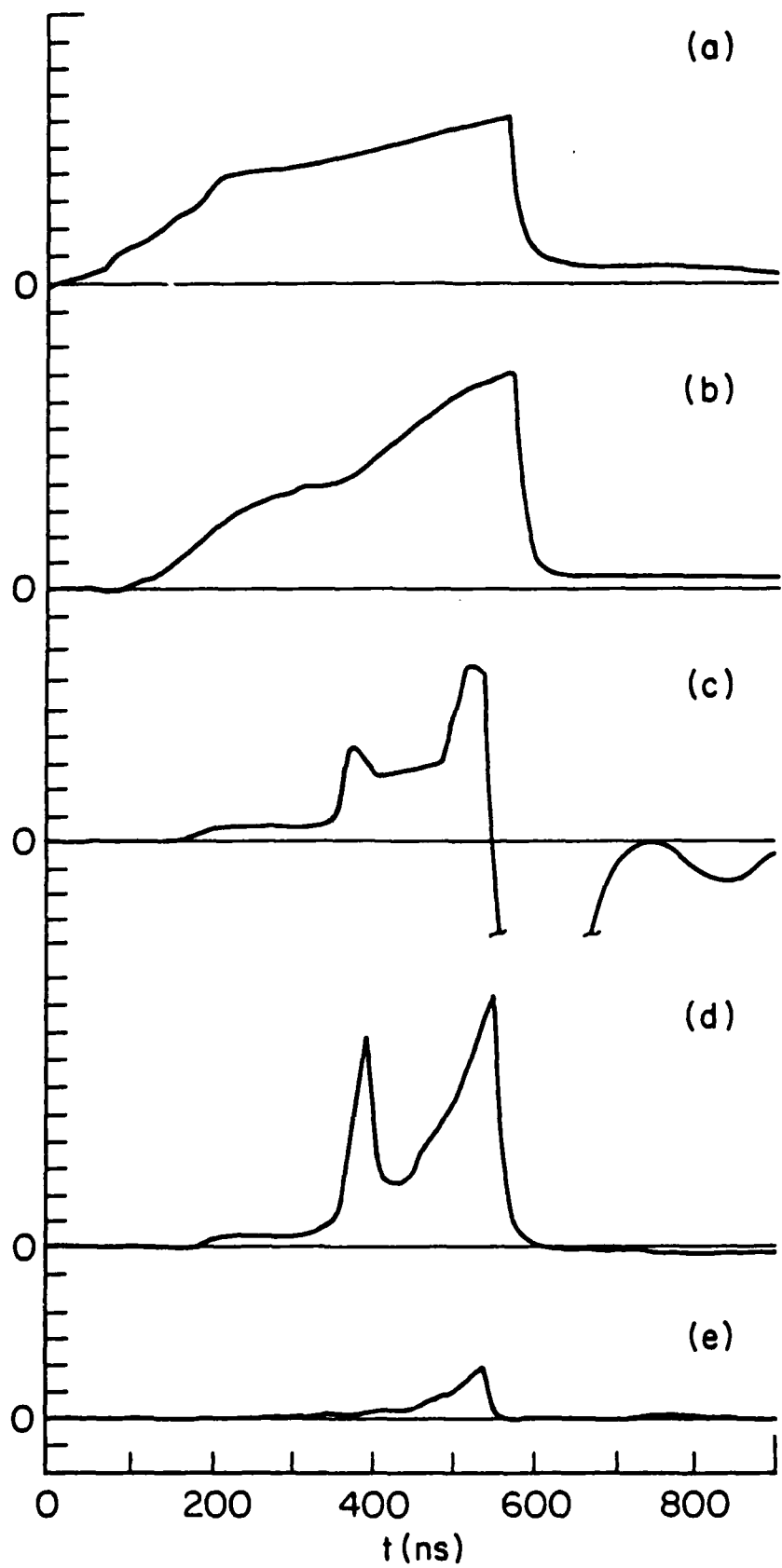


Figure 10

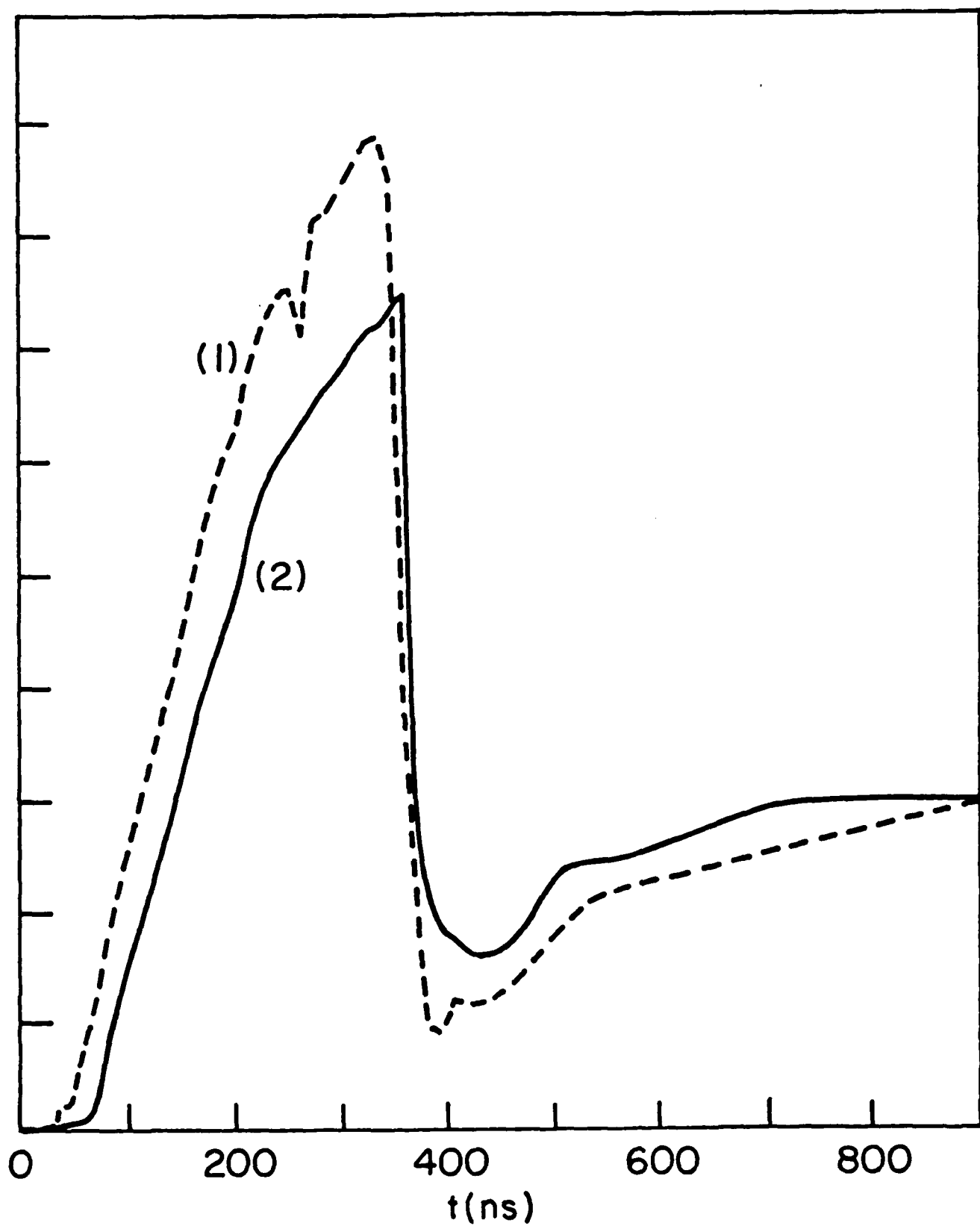


Figure 11

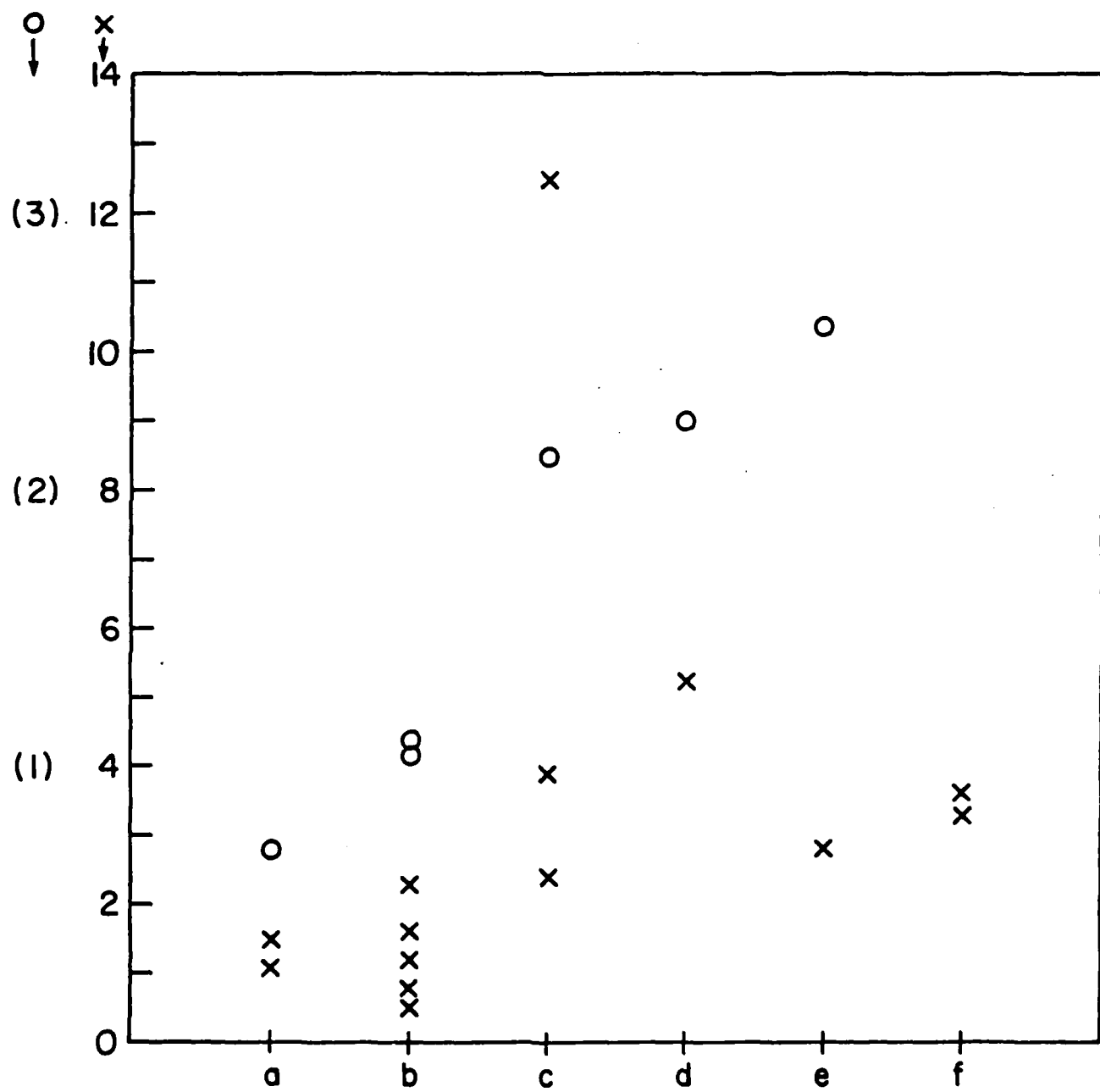


Figure 12a

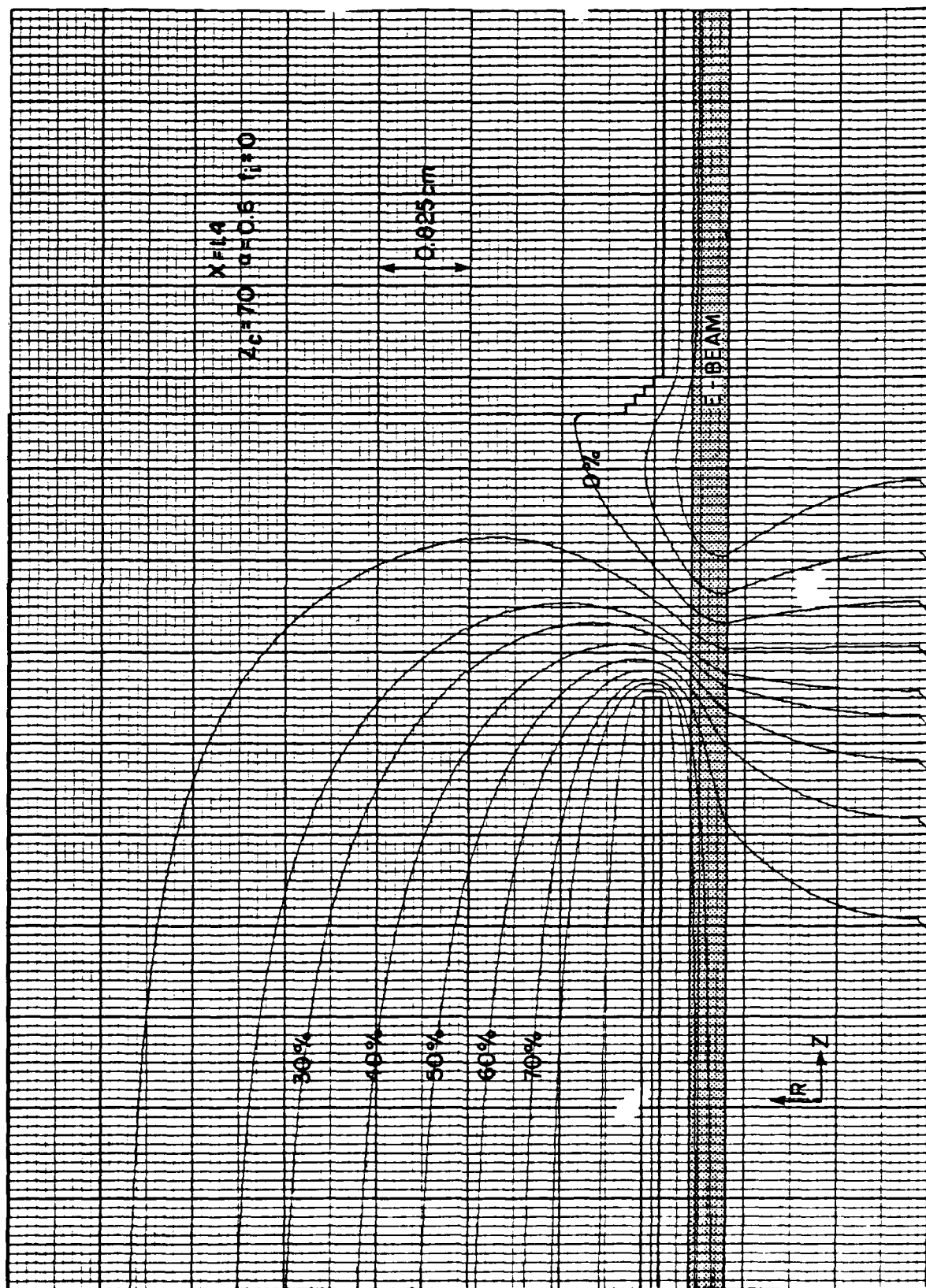


Figure 12b

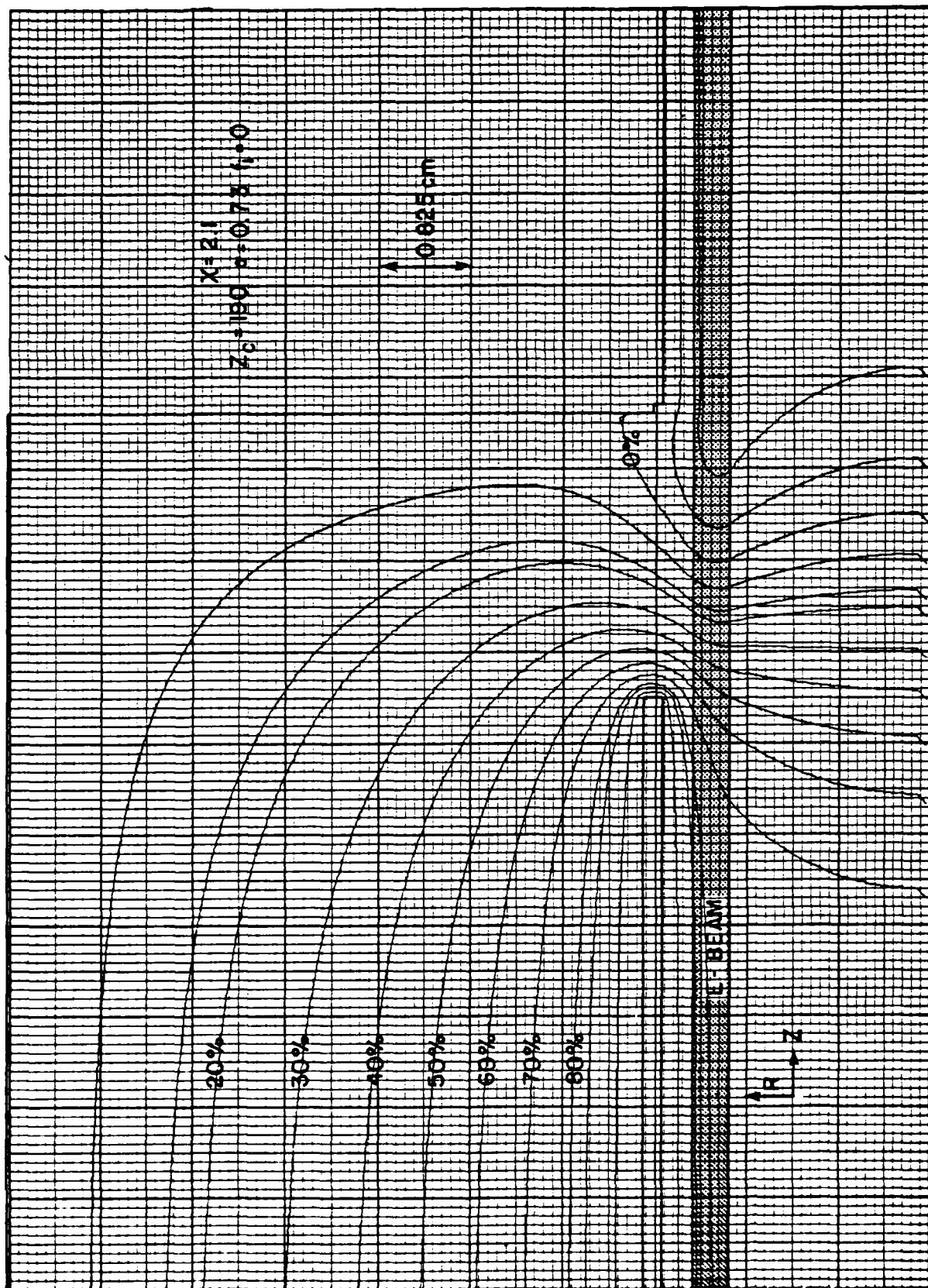


Figure 12c

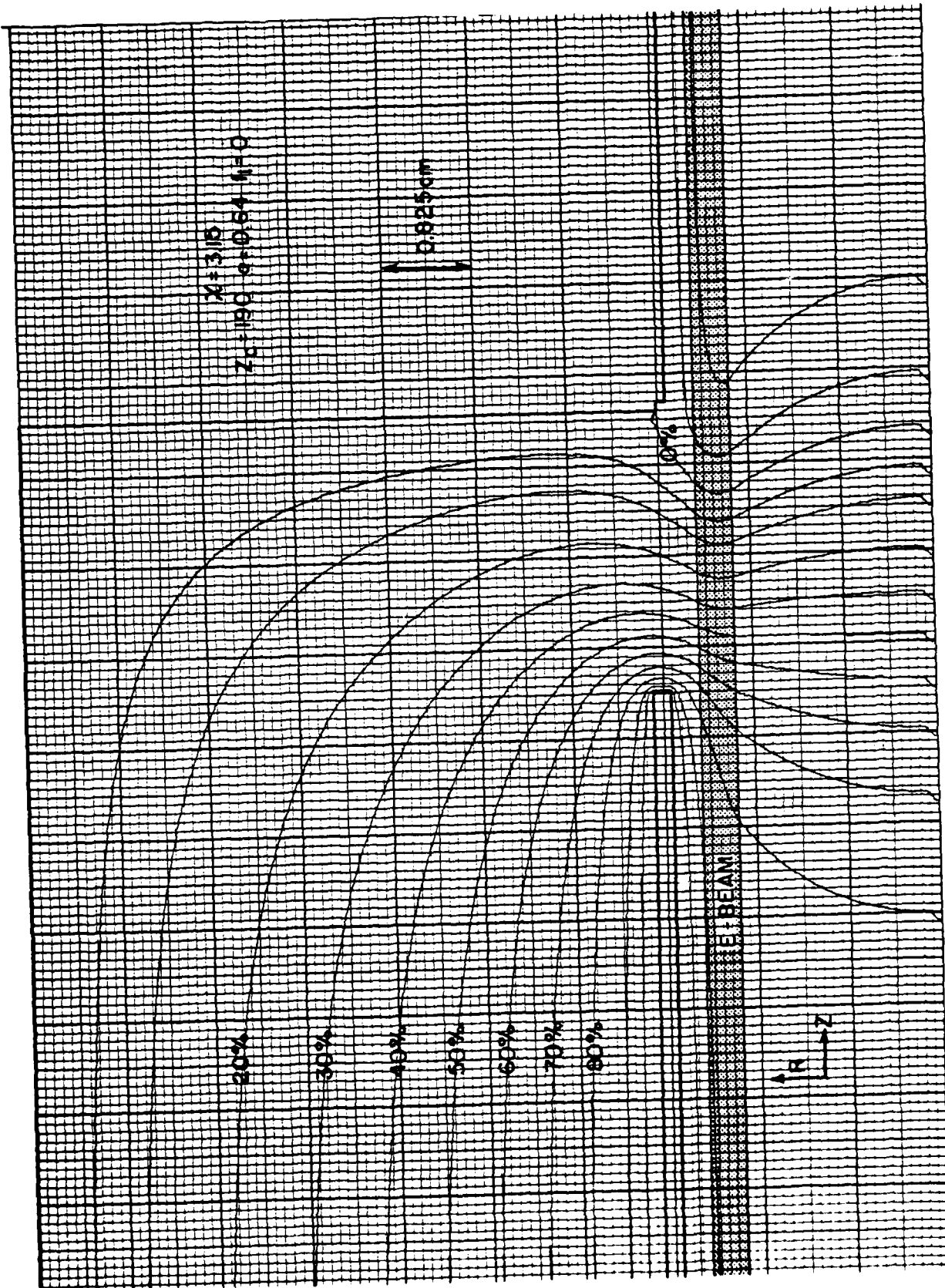


Figure 12d

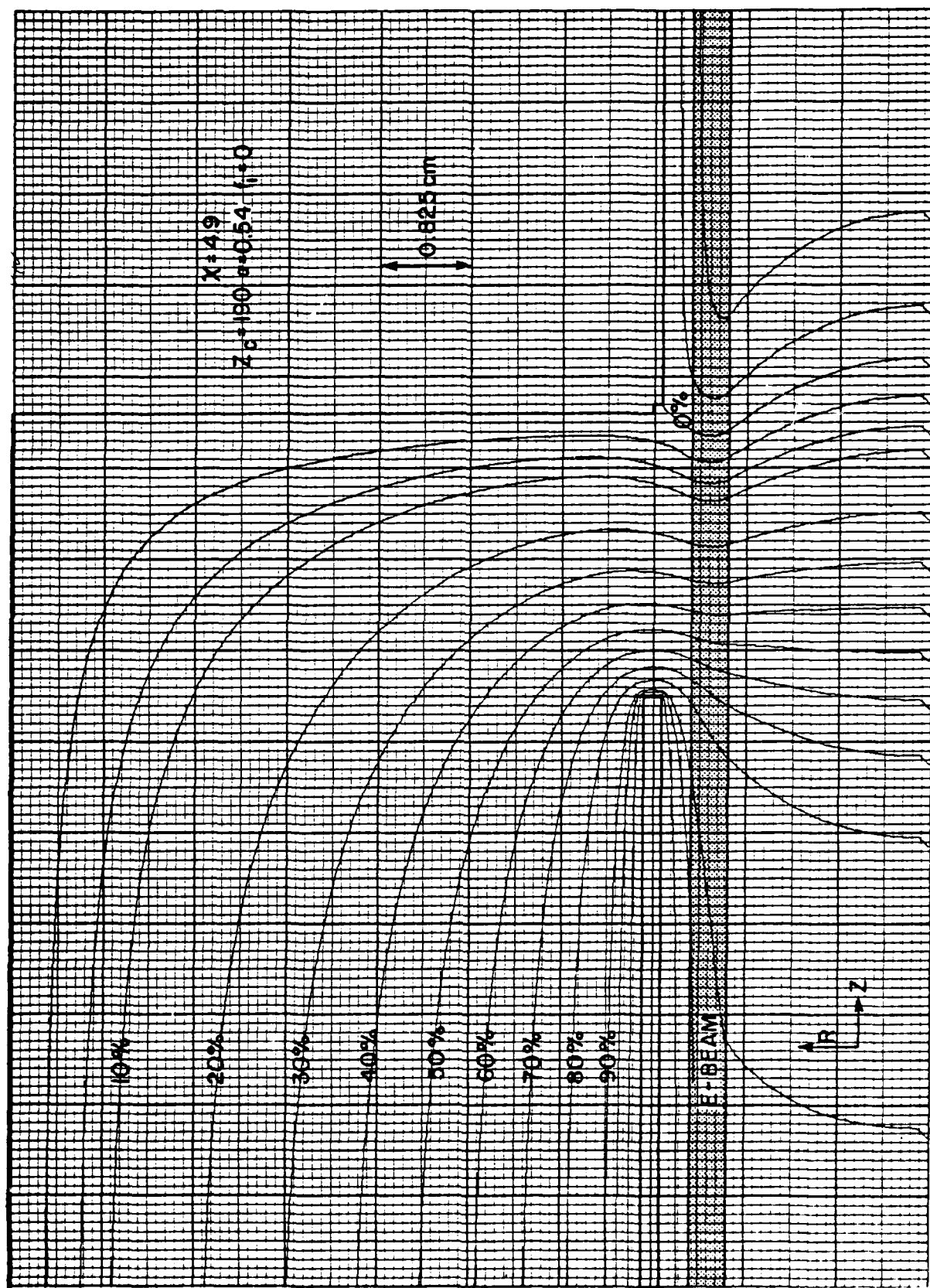


Figure 12e

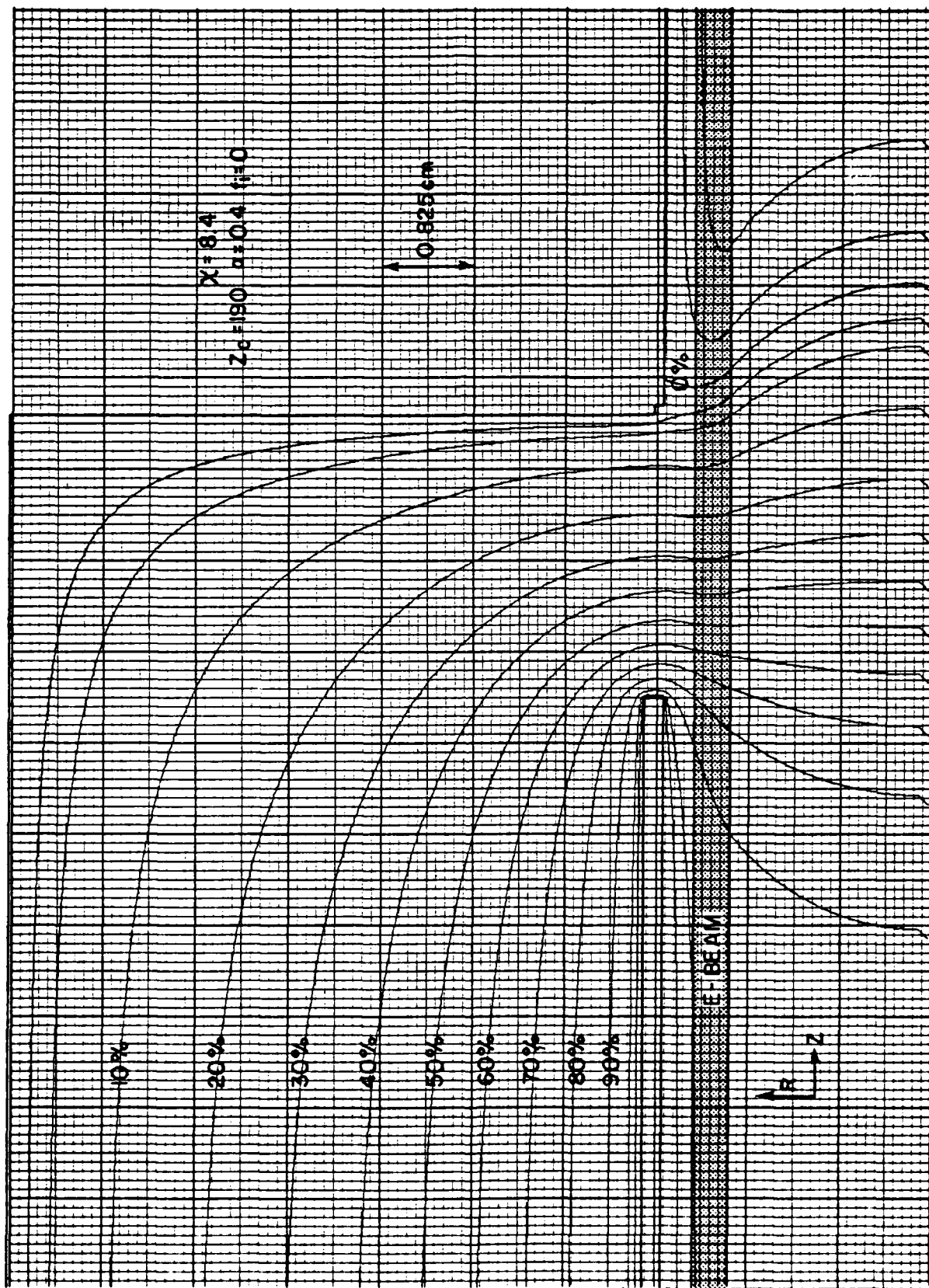


Figure 13a

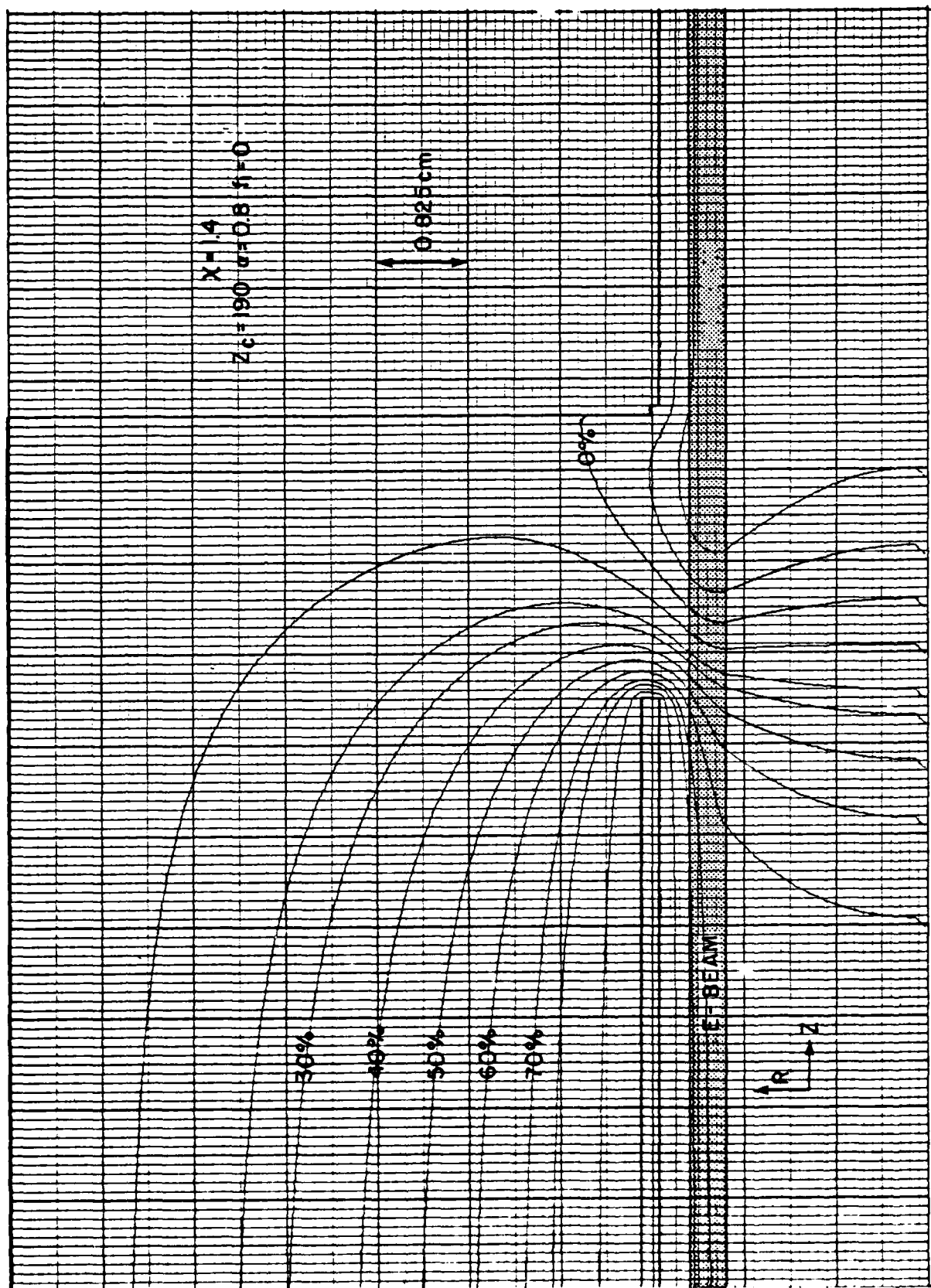


Figure 13b

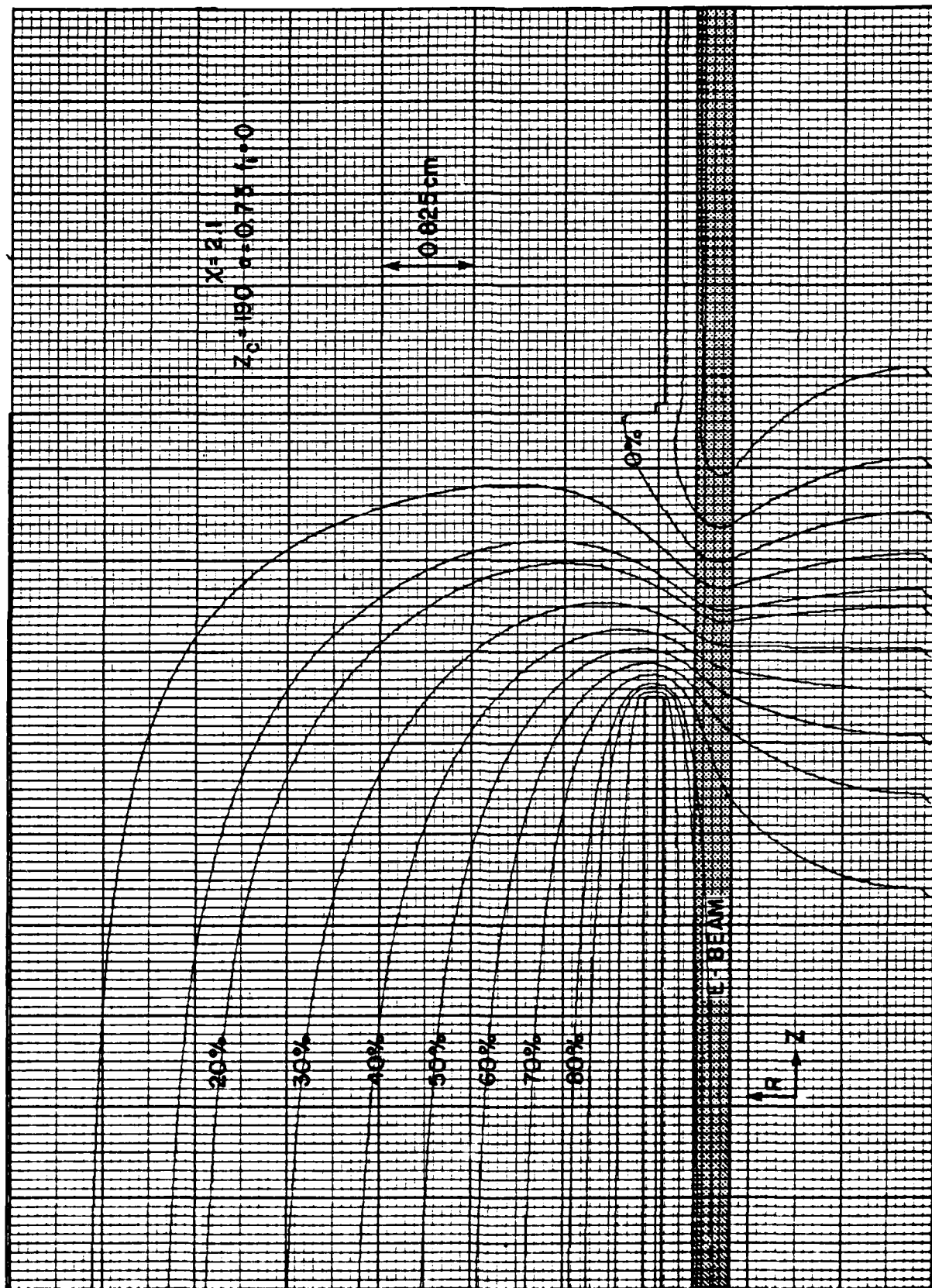


Figure 13c

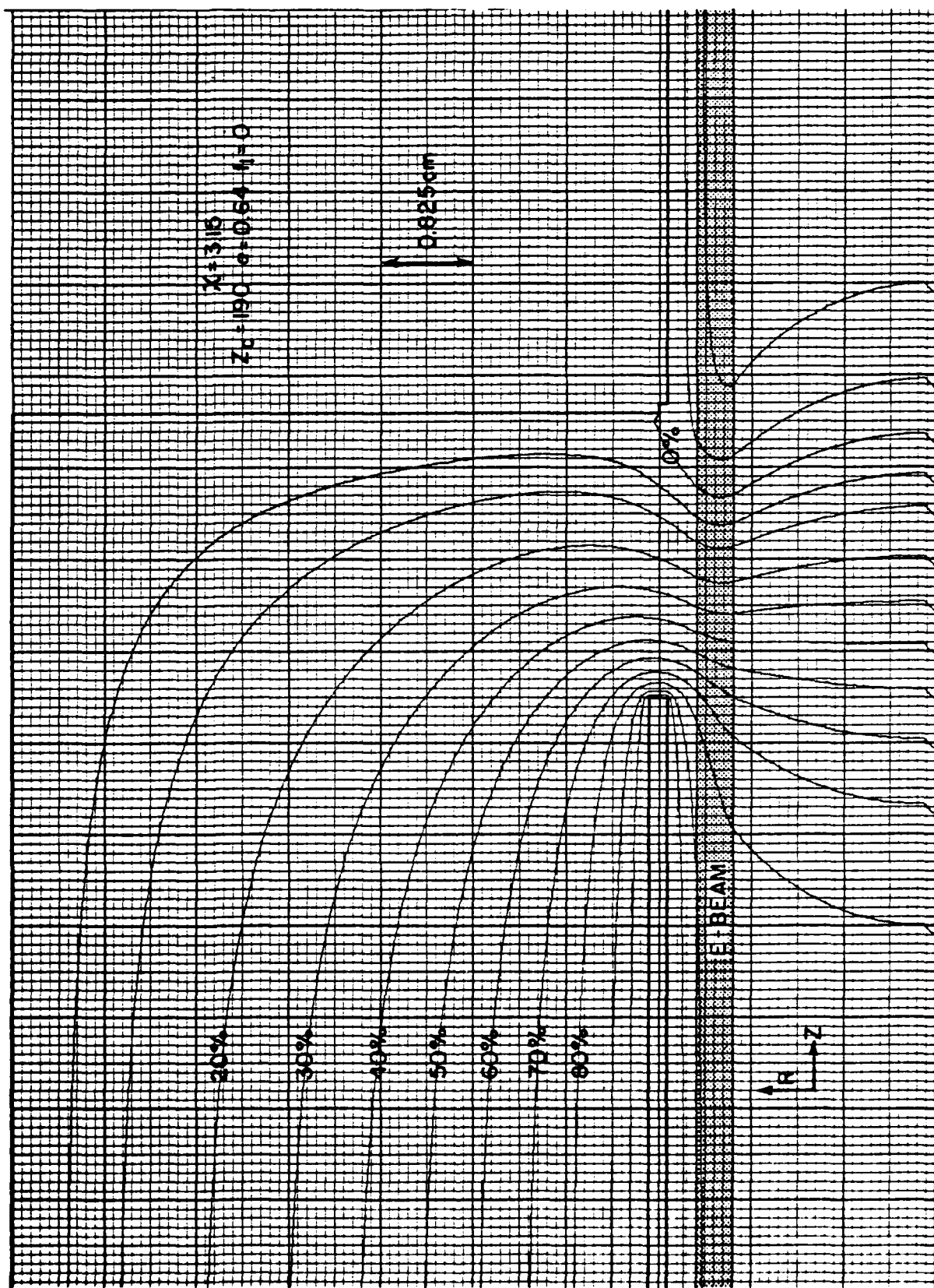


Figure 13d

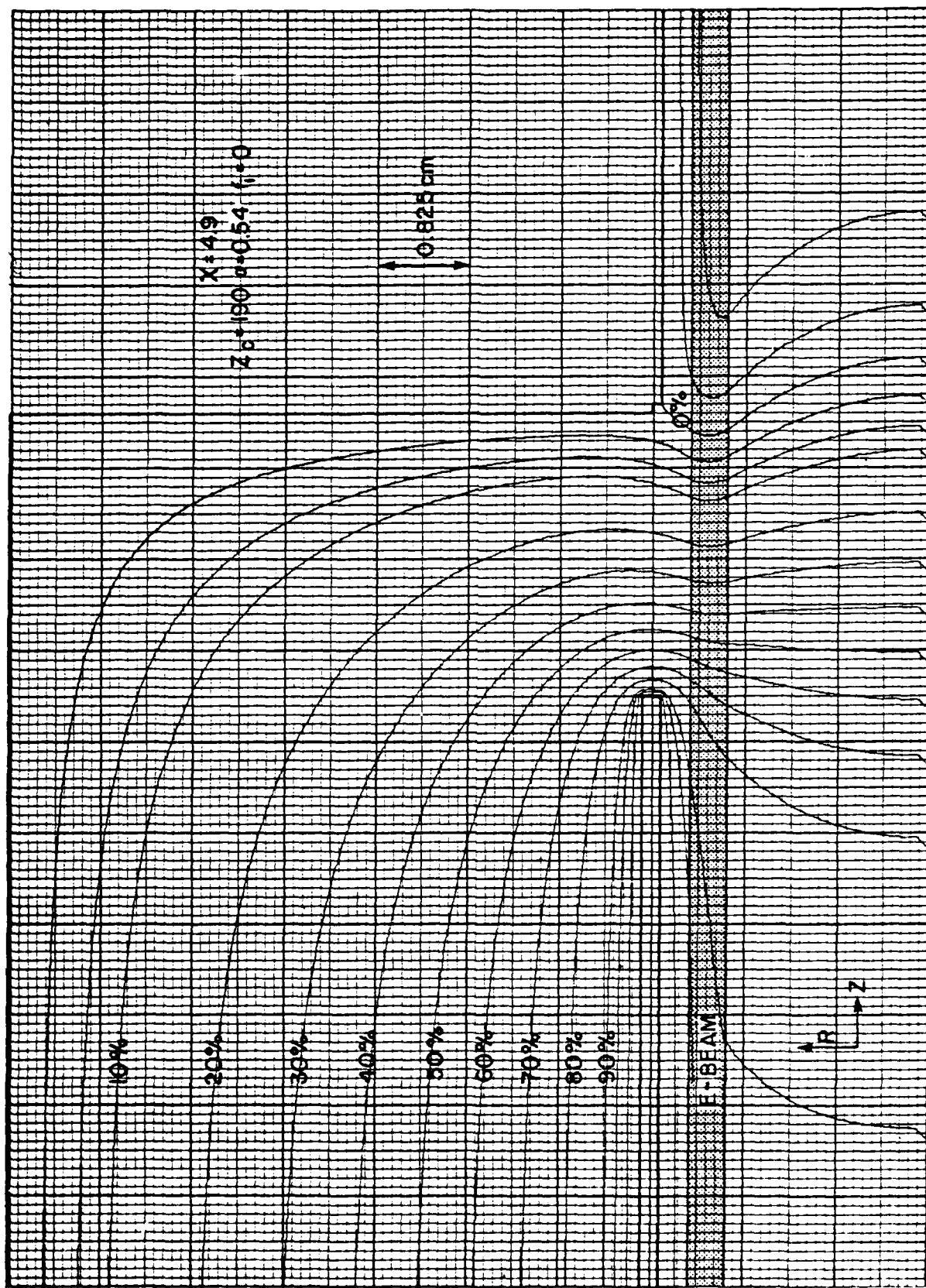


Figure 13e

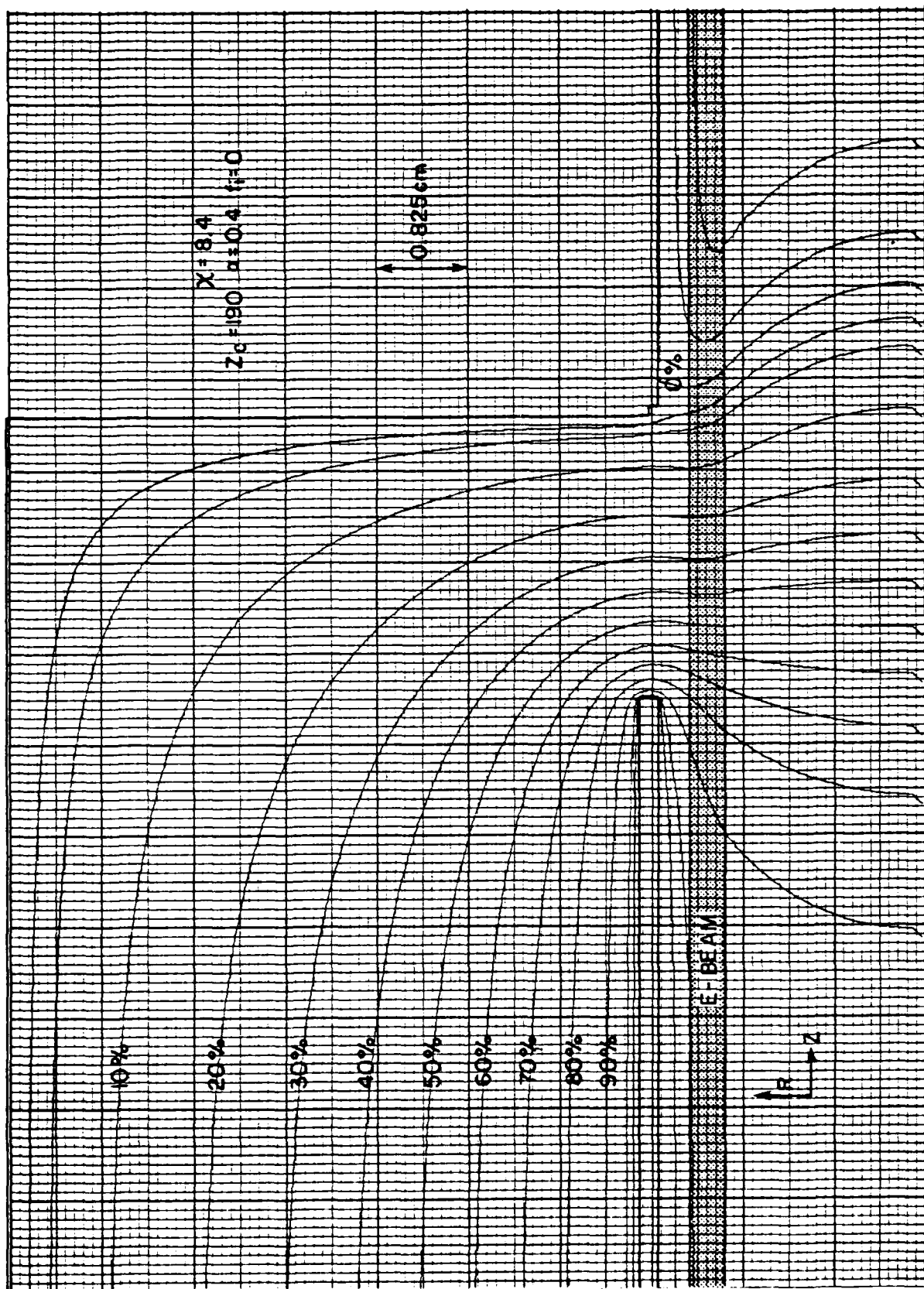


Figure 14

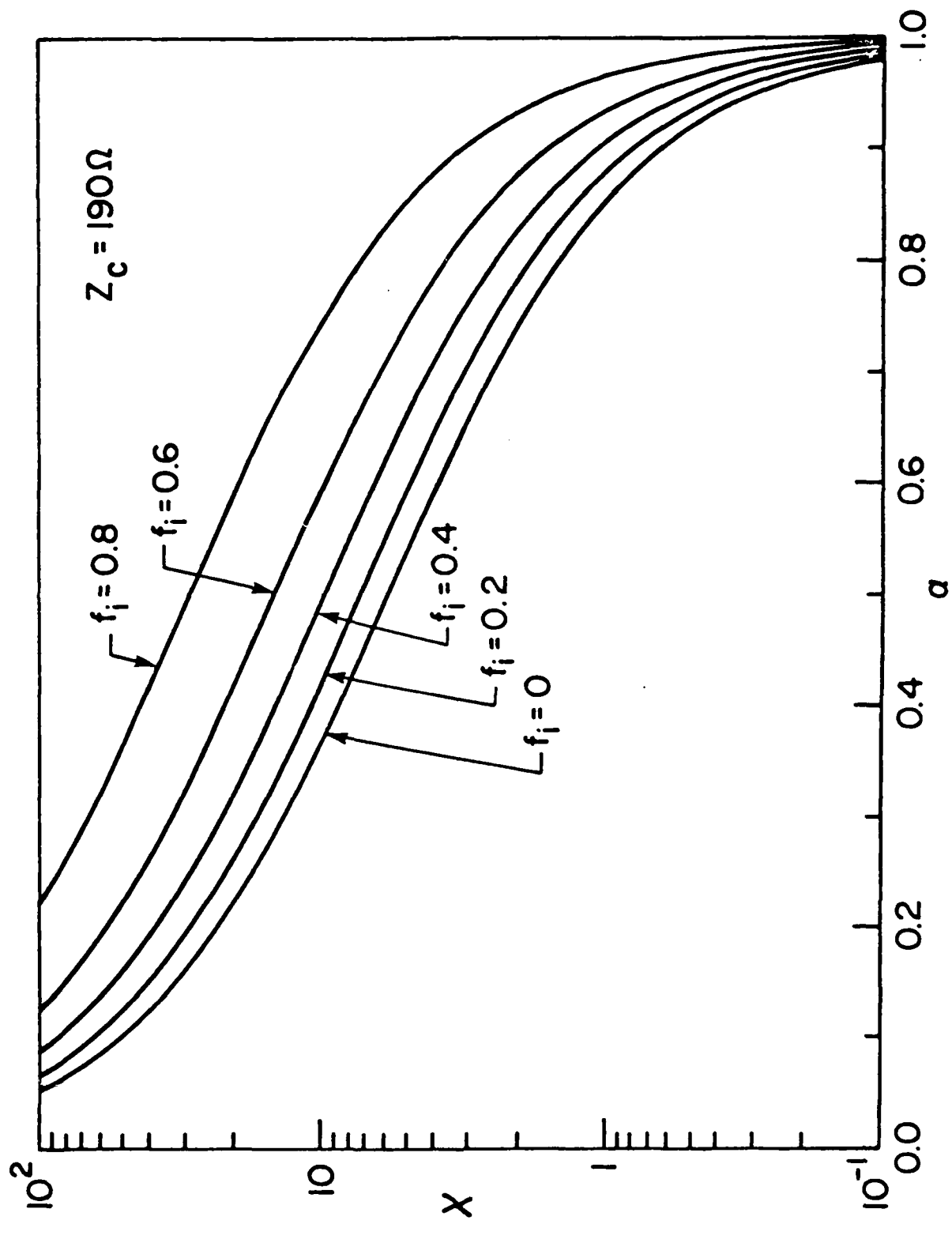


Figure 15

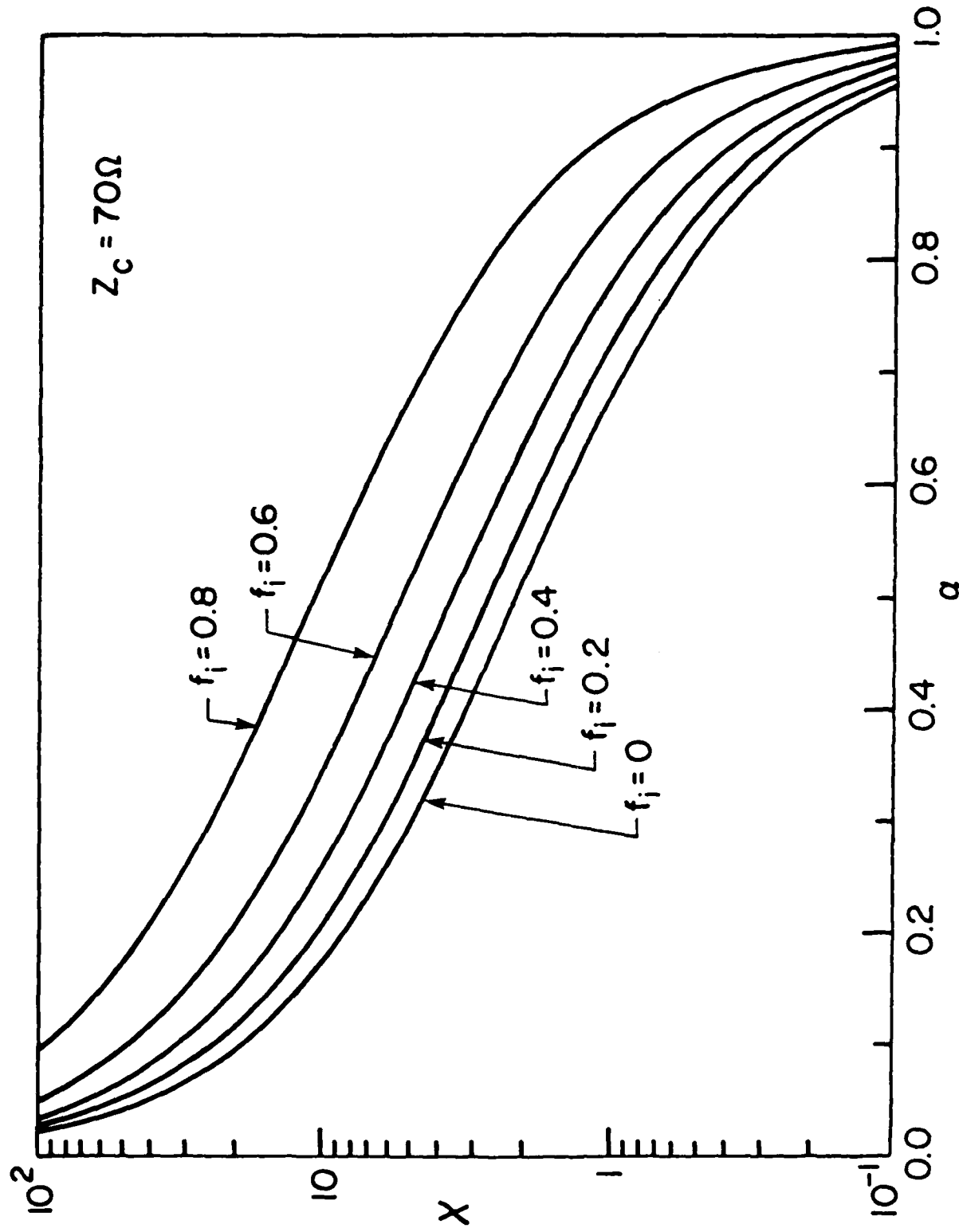


Figure 16

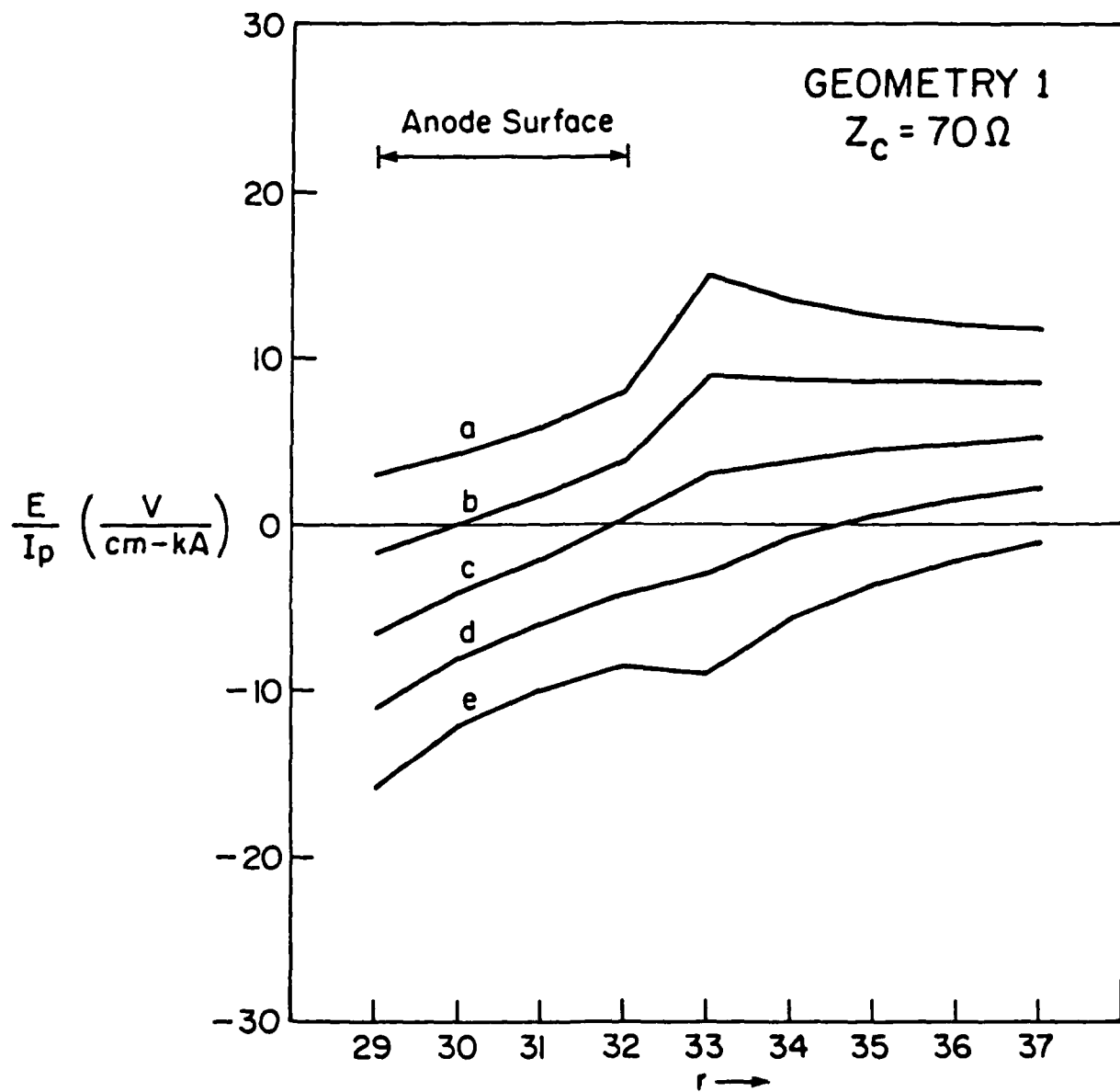


Figure 17

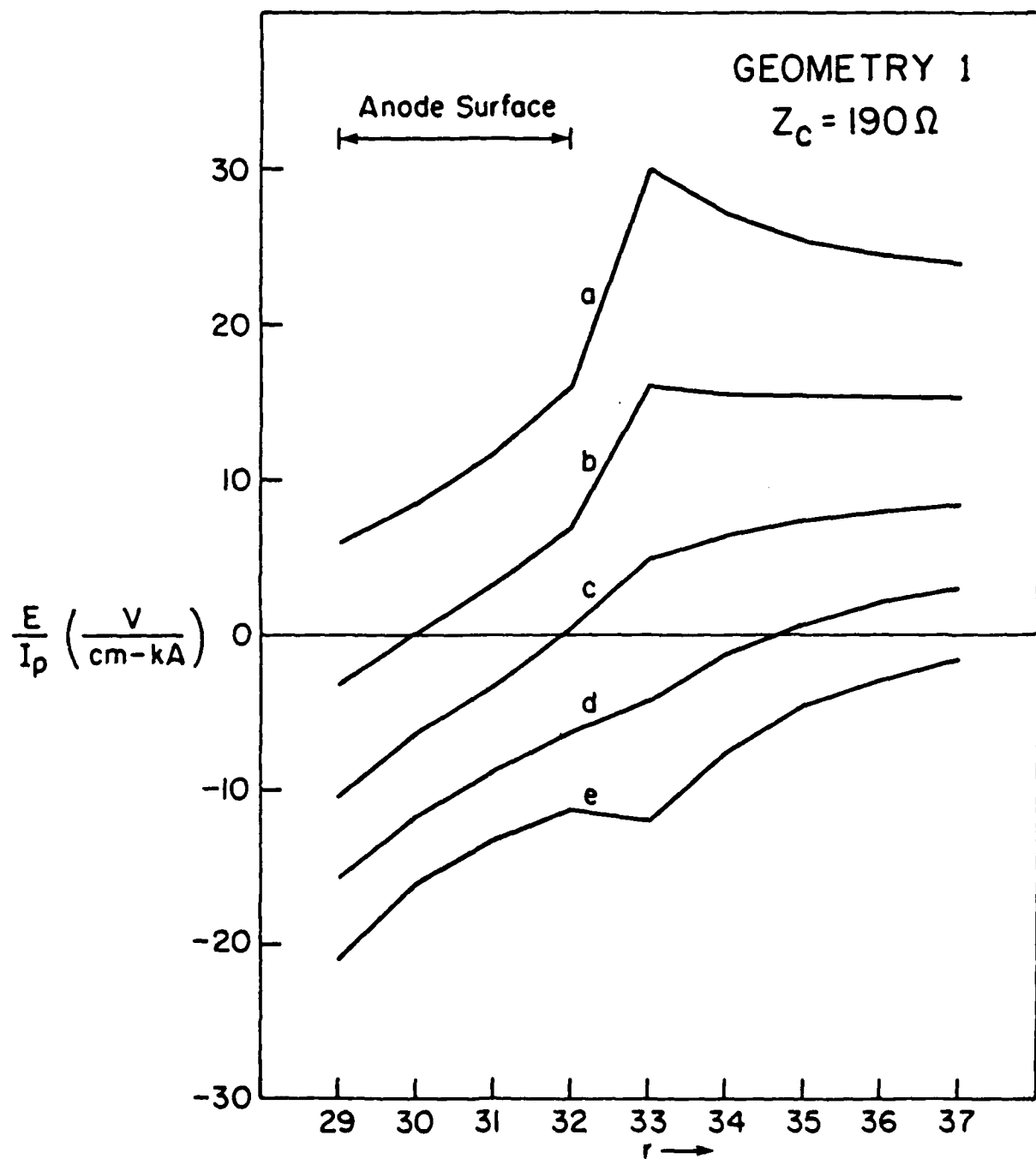


Figure 18

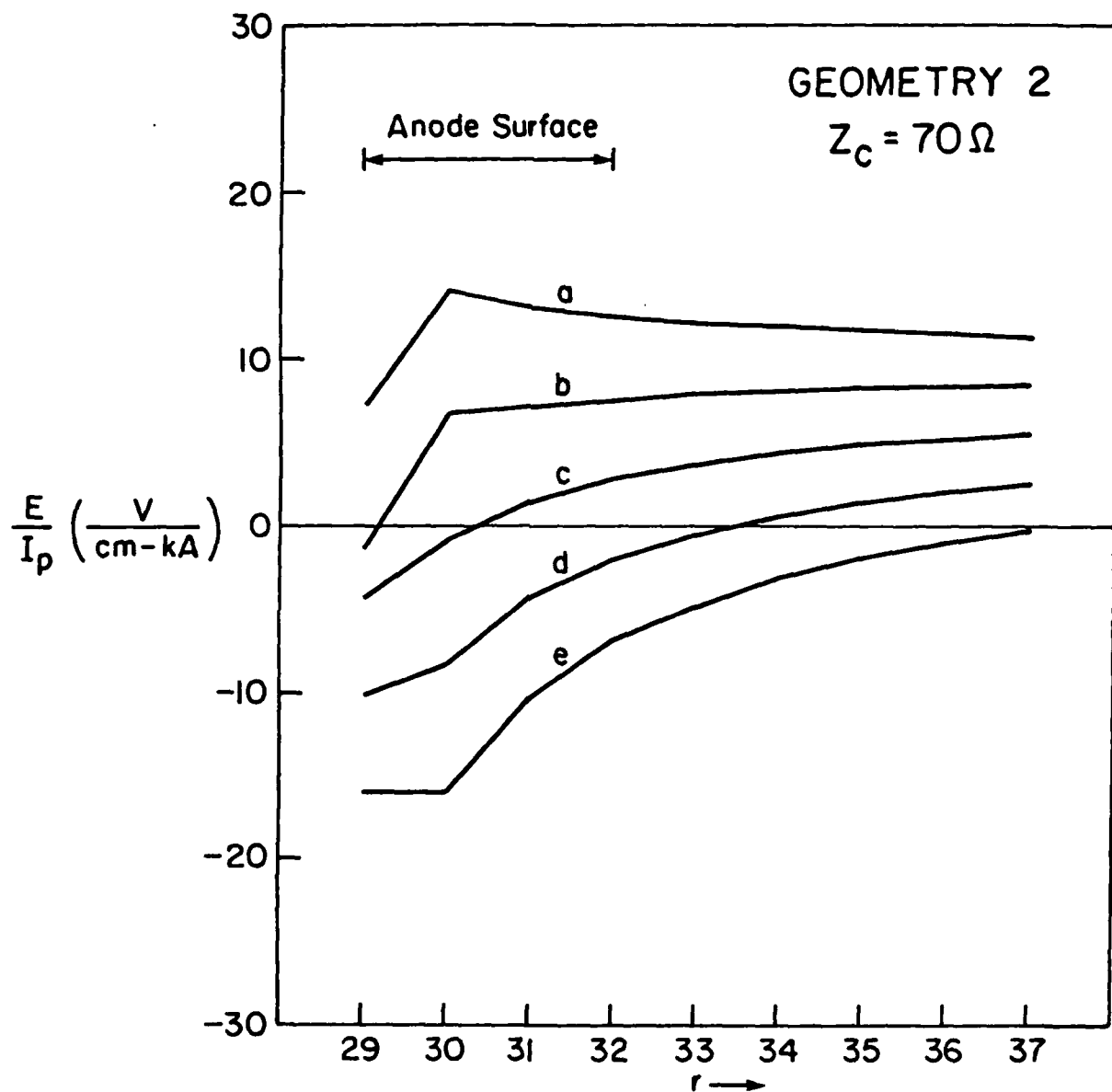


Figure 19

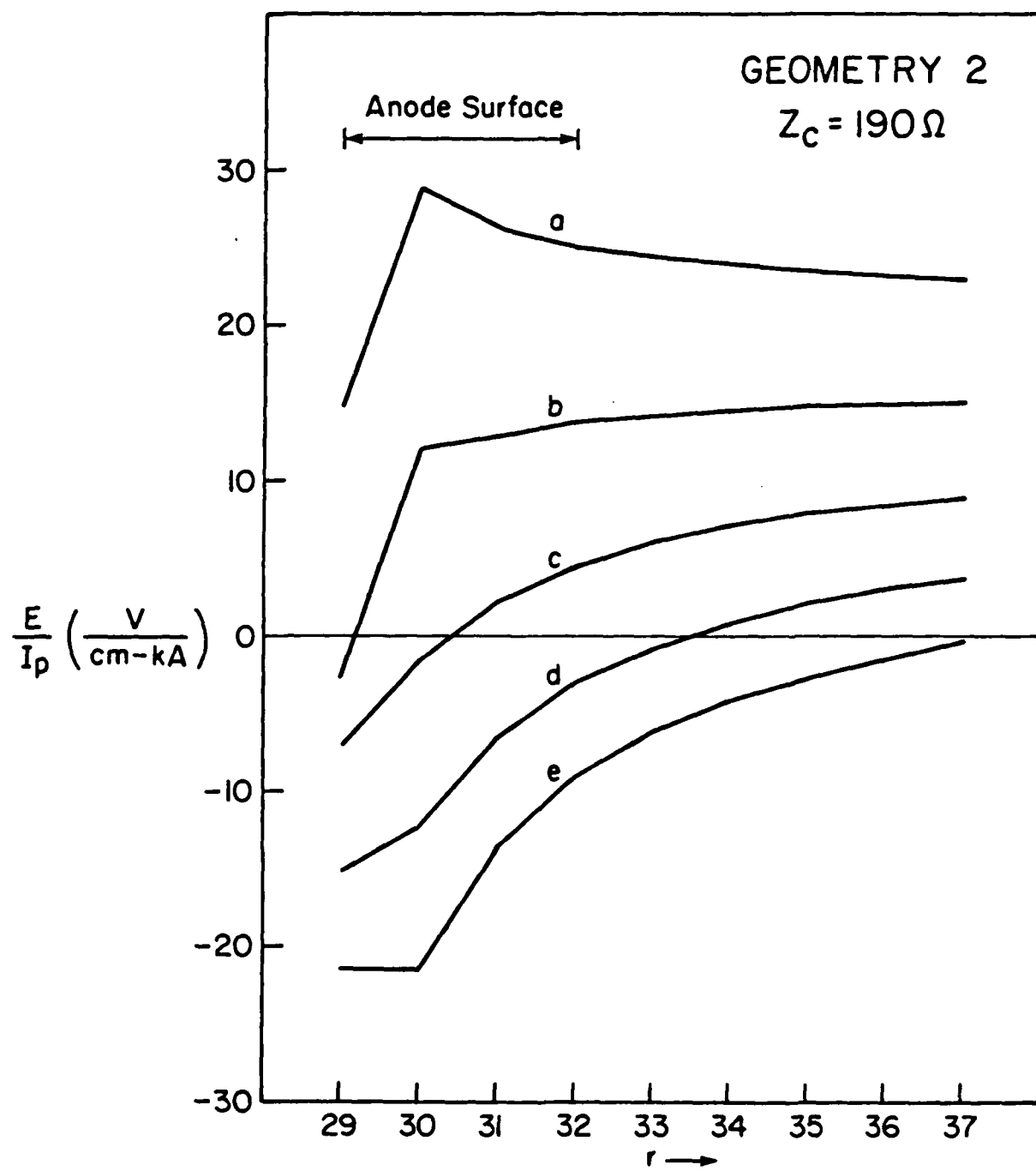


Figure 20

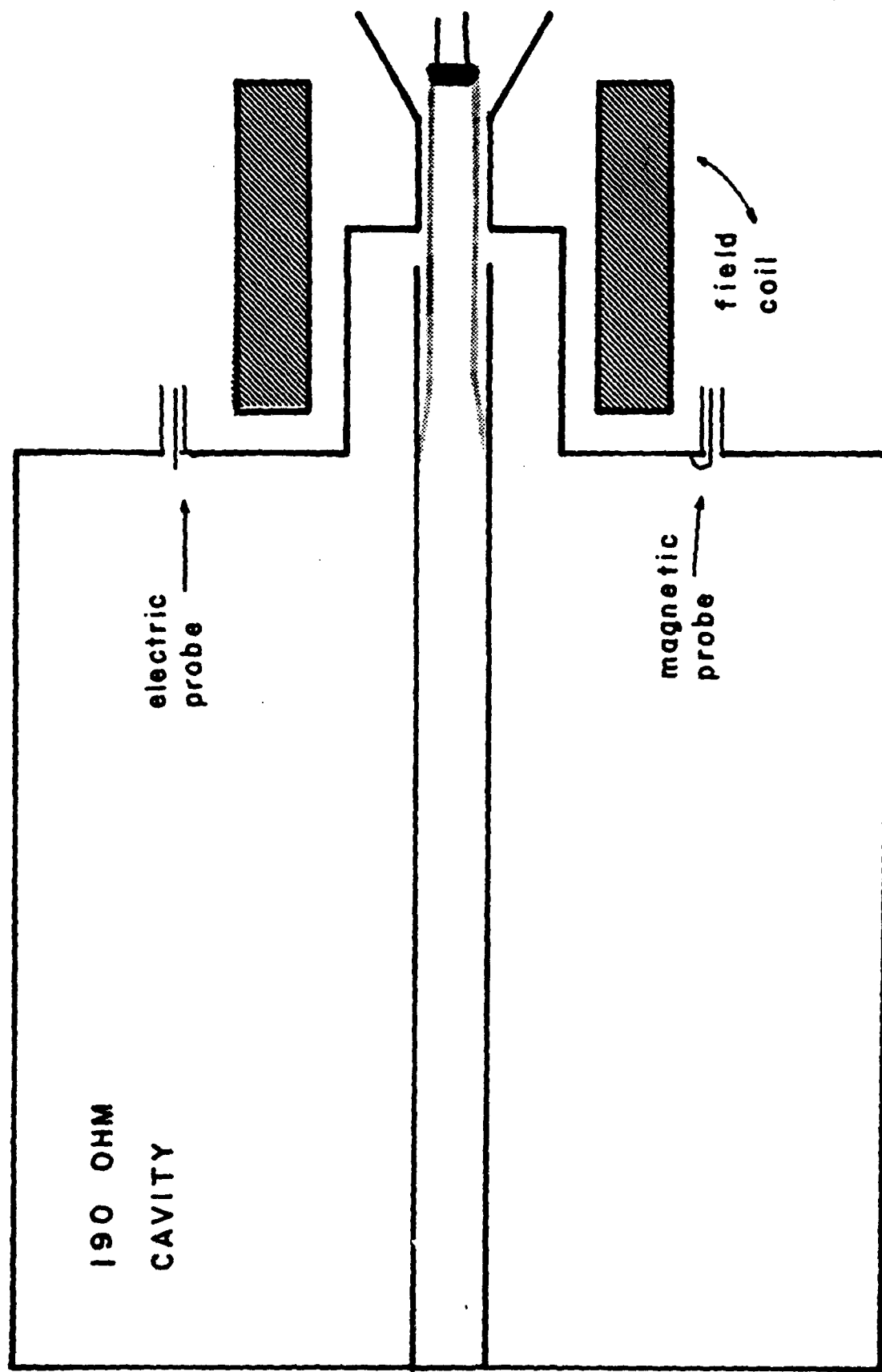


Figure 21

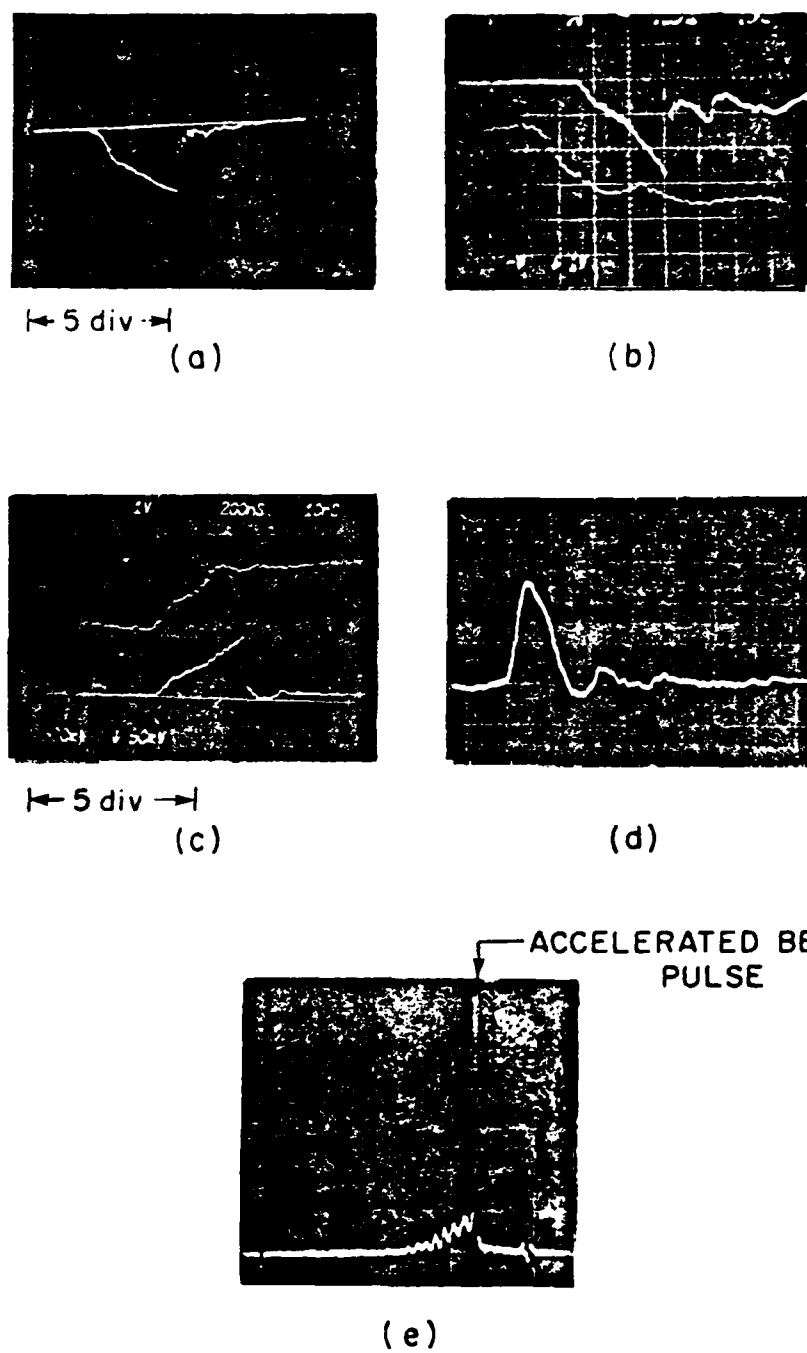


Figure 22

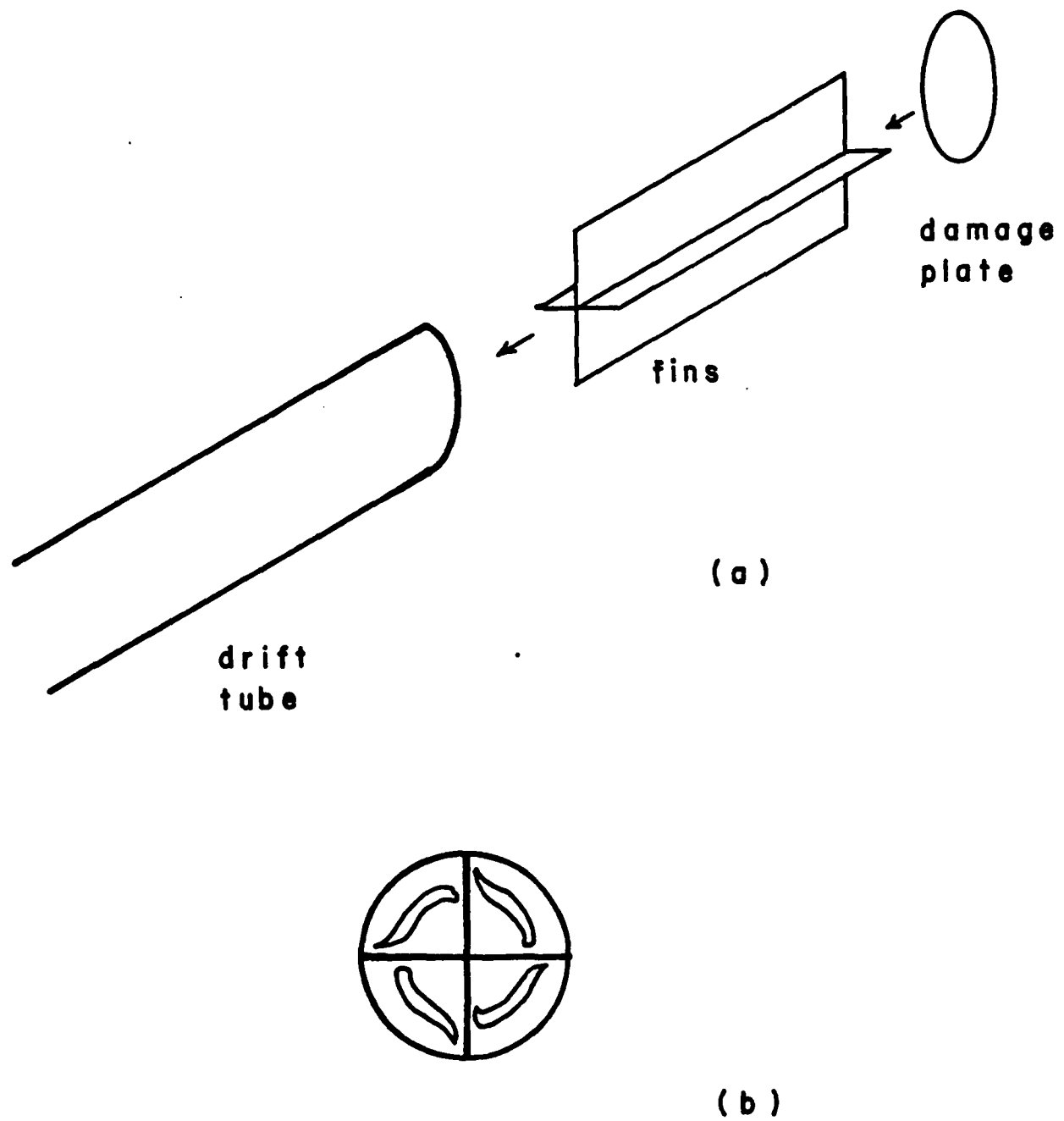
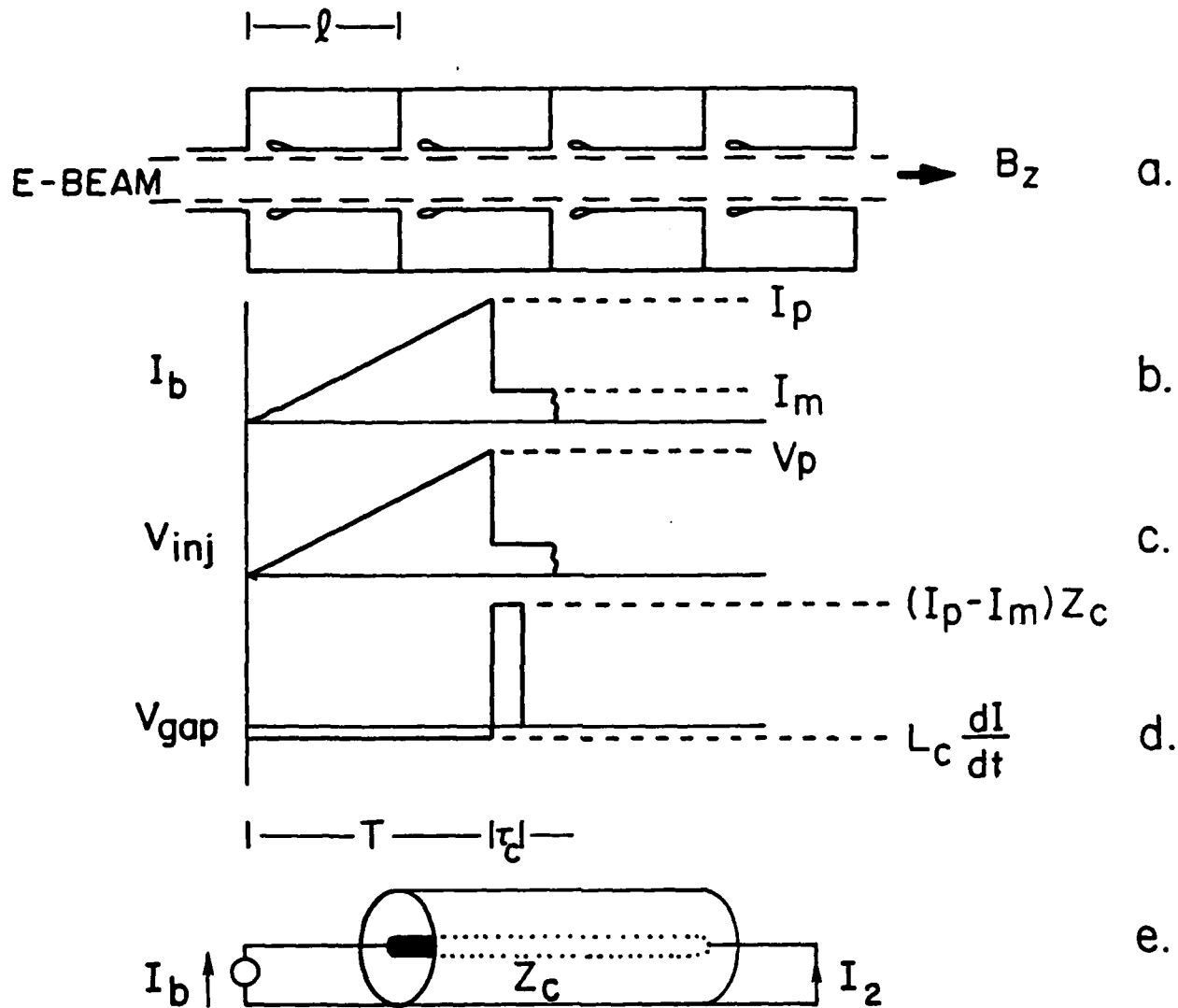


Figure A1



CURRENT SOURCE    TRANSMISSION LINE    SHORT

$T = \text{CURRENT RISE TIME} = 800\text{ ns}$

$$\tau_c = \frac{2l}{c} = 6\text{ ns}$$

$Z_c = \text{CAVITY IMPEDANCE} = 70 \Omega$

$L_c = \text{CAVITY INDUCTANCE} = 0.23 \mu\text{H}$

